STABILITY OF STRUCTURES SUBJECTED TO

ECCENTRIC LOAD IMPERFECTIONS

By

JAMES ALAN HOFFMAN
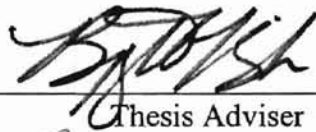
Bachelor of Science

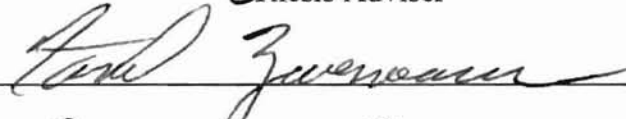Oklahoma State University

Stillwater, Oklahoma

1994

Submitted to the Faculty of the
Graduate College of the
Oklahoma State University
in partial fulfillment of
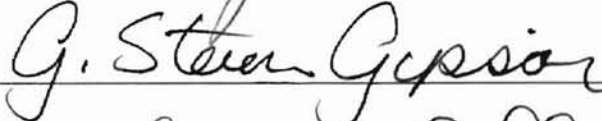the requirements for
the Degree of
MASTER OF SCIENCE
December 1996

STABILITY OF STRUCTURES SUBJECTED TO

ECCENTRIC LOAD IMPERFECTIONS

Thesis Approved:

_____
Thesis Adviser

_____

_____

_____
Dean of the Graduate College

ACKNOWLEDGMENTS

I would like to thank my advisor, Professor Bjong Yeigh for his seemingly inexhaustible patience, good humor, insights, and guidance as I struggled through the mathematics, potential energy formulation, and the many tiring hours of computer simulation. I was constantly amazed at his capacity to tackle great volumes and varieties of work at the same time and still be able to crack a joke.

I would also like to thank Edward Sturm (OSU '58), and Sturm Engineering Company, for their support, encouragement, interest, and especially their tolerance. Over the last two years, my work schedule was in a constant state of chaos and I know it was often impossible to keep track of me.

Finally, and most important of all, I would like to thank my beautiful and loving wife Stacy (OSU '94). She has put up with me through the whole process. She knows how hard it was to always keep me motivated when the going got tough. This thesis is more the result of her efforts than of mine.

TABLE OF CONTENTS

LIST OF TABLES

LIST OF FIGURES

OKLAHOMA STATE UNIVERSITY

NOMENCLATURE

A	cross-section area
E	elastic modulus
EI	bending rigidity
$(EI)_o$	bending rigidity (mean value)
K	foundation stiffness
φ	non-dimensional foundation stiffness
φ_o	non-dimensional foundation stiffness (mean value)
L	beam length
L_p	modified beam length
M	number of generalized coordinates
N	number of imperfection modes
G_{ff}	one-sided power spectral density function
G_{fofo}	non-dimensional one-sided power spectral density function
R_{ff}	autocorrelation function
R_{fofo}	non-dimensional autocorrelation function
P	applied axial load
V	total potential energy function

v	non-dimensional total potential energy function
W	lateral deflection
w	non-dimensional lateral deflection
$w_o(x)$	non-dimensional initial shape deformity
X	axial coordinate
x	non-dimensional axial coordinate
$X^{\bullet}$	fixed spatial coordinate
a, b, c, d	coefficients of the potential energy expansion
d_e	depth of the beam
b_f (f = e, k, h)	correlation distance
b_{fo} (f = e, k, h)	non-dimensional correlation distance
e_j, k_j, h_j	amplitude of imperfection pattern
e(x)	bending rigidity imperfection pattern
h(x)	shape imperfection pattern
$h^{\bullet}(x)$	shape imperfection pattern fitted to boundary conditions
k(x)	foundation stiffness imperfection pattern
j, k, l, m	mode order subscripts
q	generalized coordinates
r	inverse geometric stiffness matrix
t	radius of gyration
γ	coefficient of the eigenvalue problem
δ_{jk}	Kronecker Delta
δ_q	virtual change in the generalized coordinate q

δV	first variation of the potential energy
δv	non-dimensional first variation of the potential energy
$\delta^2 V$	second variation of the potential energy
$\delta^2 v$	non-dimensional second variation of the potential energy
ε	universal imperfection magnitude
ε_{cr}	critical imperfection magnitude
ε_{RMS}	root mean square critical imperfection magnitude
η	eccentricity in the applied load
κ	wave number
κ_u	upper cut off wave number
κ_{uo}	non-dimensional upper cut off wave number
ξ	maximum magnitude of shape imperfection
ρ	non-dimensional buckling load of the actual structure
ρ_{cl}	non-dimensional classical buckling load of the actual structure
σ_f $(f = e, k, h)$	standard deviation for $f(x)$
σ_{fo} $(f = e, k, h)$	non-dimensional standard deviation for $f(x)$
σ_η	non-dimensional standard deviation for η
Φ	random phase angle

CHAPTER I.   *Introduction*

One of the last fundamental frontiers that remains to be fully explored in structural engineering is the phenomenon of buckling in slender, imperfect columns. Generally, columns are any element in a structure that transfer compressive loads. Unlike tension and flexural members that fail when the applied loads cause stresses that exceed certain material limitations, slender columns most often fail by buckling. Furthermore, column buckling does not depend on the proportional limit of the member. Buckling is a complex failure mechanism that is often catastrophic with little or no warning. It depends not only on the material and section properties of the column, but also on the contributions and interactions of its length, end support conditions, lateral supports, and location of the applied load.

For many years, the prediction of the buckling load in columns has been based on classical stability analysis [Timoshenko and Gere 1961, Thompson and Hunt 1973 and 1984]. The current stability theory is actually developed largely from the work of Leonhard Euler who first analytically investigated the column buckling phenomenon in 1744.

Over the years, little has been done beyond extending and refining Euler's work. By 1926, when the first edition of the AISC Manual of Steel Construction was published, no less than 20 different variants of the Euler column buckling formula were in general use among steel designers alone. These were all given as examples by the Manual, merely as suggestions from which to choose [AISC 1926]. These, and other buckling formulations based on the Euler equation had some rational consideration for the

behavior of the material in question. They all perform empirically well for ideal columns with concentric loads, and models that are not unusually sensitive to imperfections.

However, everything is imperfect, and structures are no exception. Structural imperfections are defined as any small, unavoidable deviations from the perfect structure. These deviations include those of shape (i.e., initial curvature), material properties, section properties, support mechanisms, and the geometric configuration of the applied load such as accidental eccentricity. In other words, the "perfect" structure is differentiated from the "actual" structure in that it has no imperfections of any kind.

While not all structures are sensitive to imperfections, experience and experimentation have shown that the buckling load of some structures are quite sensitive to structural imperfections [Wilson and Newmark 1933]. Currently, imperfections are usually dealt with in design work by increased factors of safety, which are known to engineers as "factors of ignorance." As with any blind factor of safety (i.e., a safety factor used to account for reasons that can not be analyzed in a rational or known way), the result is more often than not excessive overdesign and waste. This is because until only quite recently there have been no reliable tools or methods to determine to what degree imperfections affect buckling loads.

For the most part, engineers approach imperfections by using some rational means to determine the stresses in a column that are caused by the imperfection, and then checking this against the Euler load, possibly with an added safety factor. That is, the stresses caused by imperfections are calculated first, and then the capacity of the column without imperfections is computed. Finally, a safety factor is assigned based on the analyst's experience, rule-of-thumb, and common sense. However, safety factors on the

2

Euler load are not a rational answer to imperfection sensitive buckling (especially if one is unable to determine how sensitive the structure is to imperfections in the first place).

For example, in an attempt to more accurately analyze the effect of shape imperfections, engineers have occasionally resorted to the methods that involve the secant formula in order to capture the effects of the imperfection [Timoshenko and Gere 1984]. The modified secant formula for shape imperfections is:

$$\sigma_{max} = \frac{P}{A}\left[1 + \frac{\frac{\xi c}{t^2}}{1 - \frac{P}{\pi^2 EA}\left(\frac{L}{t}\right)^2}\right] \qquad (1.1)$$

where σ_{max} is the maximum stress in the column, P is the applied load, A is the cross sectional area, L is the column length, E is Young's Modulus, t is the radius of gyration, c is the distance from the centroid to the extreme fiber (on the concave side) and ξ is the maximum magnitude of the shape imperfection. The term $\frac{\xi c}{t^2}$ is known as the imperfection ratio.

While the secant formula will give good results for the stresses in a column with imperfections, it is not a buckling formula. It is a strength formula. For the determination of the buckling load, the secant formula is quite useless. The formula gives an excellent estimate of the stress in the column, but it does not and cannot predict whether or not the column has survived up to the classical buckling load. Furthermore, it does not say if the structure is sensitive to imperfections.

If a structure is insensitive to imperfections, stable equilibrium exists at the critical load [Timoshenko and Gere 1961]. See *Figure 1.1*. All neighboring equilibria exist for

3

loads equal to the critical load (in the case of *Figure 1.1*), and greater than the critical load in the more general case.
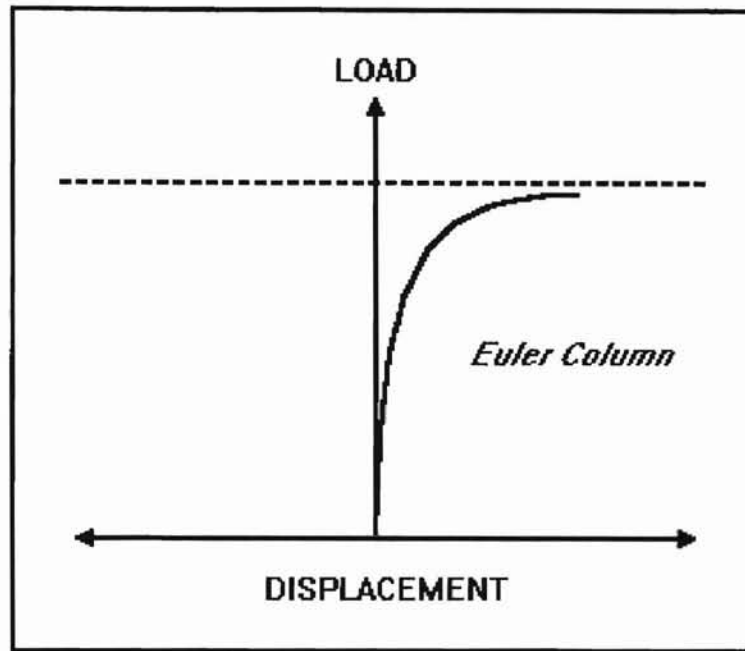
Figure 1.1: Buckling response of imperfection insensitive structure.

Examples of structures that are insensitive to imperfections are simply supported beams, Euler columns, the elastica, etc.

However, if a structure is sensitive to imperfections, an unstable equilibrium exists at the critical load, and it is possible for neighboring equilibria to exist at loads less than the critical load. The structure may experience structural "softening" as it nears the critical load and consequently less load is required to produce more deflection [Bazant and Cedolin 1991]. See *Figure 1.2*. After the critical load is reached, less load is required to produce additional deflection. This implies that once buckling is initiated, there is very little, if anything, that can be done to prevent a complete structural collapse

of the system. The collapse continues to progress unabated even if some of the load is removed. It also means that structural failure may occur at loads less than the classical buckling load. In some cases, the reduction in load capacity due to even relatively small structural imperfections can be as much as 50 percent [Yeigh 1995].
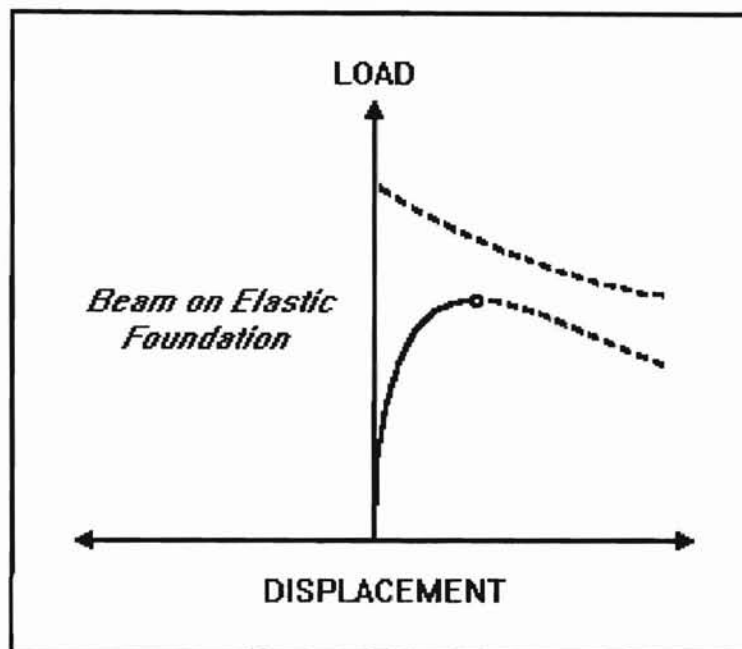
Figure 1.2: Buckling response of imperfection sensitive structure

Examples of structures that are sensitive to structural imperfections are thin shells, space frames, thin-walled beams, arches, and laterally supported columns such as the beam on elastic foundation (BEF), as shown in *Figure 1.2*.

Much research has been employed in developing methods of deterministic analysis for imperfection sensitive structures. However, gross assumptions must be made about the location and magnitude of the imperfections. More realistically, some researchers have considered the stochastic approach toward imperfections [Shinozuka and Astill

5

1971, Amazigo 1974, Elishakoff 1985 and 1988, Palassopoulos 1992, Ivanova and Trendafilova 1992]. The resulting analysis methods from these researchers treat the imperfections as random variables and attempt to determine the aggregate mean effect on the buckling stability. Unfortunately, these methods are also quite mathematically and analytically complicated. They consequently tend to be so abstract that they detract from a meaningful understanding of the physics that are involved in the buckling phenomenon.

Over the last 50 years, the developments in imperfection sensitive stability analysis have been largely incremental improvements to Koiter's dissertation. Koiter's theory approaches stability in a continuum form of an energy analysis [Koiter 1945]. However, due to various modeling assumptions and simplifications, its application is limited to shape imperfections only. At the time Koiter wrote his dissertation, only shape imperfections were considered to be significant in the classical buckling mode. Thus, if the classical buckling mode is the fourth mode, only the fourth imperfection mode can be considered. A further limitation is that Koiter's theory cannot consider any non-shape imperfections in non-classical buckling modes.

Many researchers have added to and expanded the application of Koiter's theory and many of these still consider only shape imperfections [Song and Simitses 1992, Sridharan 1994]. In addition, some work has been completed using the differential equations approach on shape imperfections [Elishakoff 1985]. These researchers are aware that other imperfections can affect the buckling stability of their structures, but have only been able to intuitively guess that shape imperfections should be dominant. Since Koiter's theory (and hence all methods that are developed from it) cannot consider non-shape imperfections, they have been unable to verify this assumption.

Finally, a breakthrough in stability analysis occurred in 1993 when Palassopoulos proposed the Critical Imperfection Magnitude (CIM) Method. This theory overcame many of the limitations and solved many of the problems associated with Koiter's theory. It is a very graceful, regular perturbation method based on the potential energy expansion of the corresponding perfect structure. Furthermore, it does not contain any limitations on the number or type of imperfections that can be considered. Consequently, the effects on buckling stability as a result of the interactions between different imperfections can now be analyzed. In his dissertation, Yeigh (1995) was the first to apply stochastic methods and CIM to study the effects and interactions of imperfections in shape, bending rigidity, and foundation stiffness.

This thesis will consider eccentricities in the applied loads among the imperfections to be modeled. The eccentricities of the applied load will vary over the sample size according to a Gaussian distribution with a zero mean.

The Gaussian distribution is meant to serve as a model for eccentric loads that are unintended, deviating from the case of the concentrically loaded beam. Here, the load is applied so as to cause no moments. But practically, it would not be possible to apply a concentric load without some deviation. According to the Central Limit Theorem, as the number of attempts to apply the load to the centerline increase, the eccentricities will asymptotically approach a Gaussian distribution.

Since CIM will play a central role in this thesis, it would be prudent to first give a brief development and description of its more salient features. It is also important to obtain an understanding of the methods that will be used to simulate the stochastic

7

imperfection patterns on the beam. CIM and simulation methods will be the subject of the next chapter.

CHAPTER II. *Critical Imperfection Magnitude Method, and*

Imperfection Simulation

Palassopoulos first introduced the Critical Imperfection Magnitude Method (CIM) in 1993. CIM is a very powerful and robust regular perturbation method that effectively replaces Koiter's Theory, which has been the premier imperfection sensitive buckling theory since 1945. Unfortunately, Koiter's Theory is very limited in the scope of its application. Perhaps its primary handicap is its inability to consider any imperfections other than those of shape.

CIM considers all types of imperfections. A new interpretation for CIM was given by Yeigh (1995) by approaching the analysis from either the load or the imperfection magnitude directions. That is, like Koiter's Theory which is only capable of determining the buckling load given a fixed magnitude of imperfection, CIM is also able to determine the magnitude of imperfection that corresponds to a given buckling load. Hence the name "Critical Imperfection Magnitude Method." In design work, engineers know what buckling load is required and would like to know what is the permissible magnitude of the many possible imperfections. CIM can be used to solve for these answers in a direct, one-time analysis.

For purposes of clarity, Palassopoulos presented his theory with only those terms up to the fourth order in the generalized coordinates, while noting that higher order terms can readily be obtained. Fortunately, most structures encountered in engineering require no more than the fourth order expansion. Also, as the number of orders is increased, the

analysis and resulting numerical computations become very complicated and mathematically ponderous. For the inextensional beam on elastic foundation (BEF) that will be considered in this study, only a second order expansion is required. What follows is a brief development of CIM. The reader is referred to Palassopoulos (1993) for a complete description of his method.

The first step in the application of CIM is to expand the potential energy of the "perfect" structure (i.e. no imperfections), V_0, in terms of the generalized coordinates q_j, $j = 1, 2, ..., M$. The variable q_j is any kinematically admissible set of generalized coordinates (e.g., buckling modes of the perfect or actual structure).

$$V_0 = v_0 + a_{0j}q_j + b_{0jk}q_jq_k + c_{0jkl}q_jq_kq_l + d_{0jklm}q_jq_kq_lq_m + \ldots \qquad (2.1)$$

The subscript, zero, indicates the perfect structure; and the coefficients $a_{(\cdot)}$, $b_{(\cdot)}$, $c_{(\cdot)}$, and $d_{(\cdot)}$ depend on the applied load, material properties, and geometric configuration of the structure. Repeated indices imply summation unless noted otherwise.

Next, the potential energy of the "actual" structure (i.e., with imperfections), V is discretized:

$$V = V_0 + \varepsilon V_1 + \varepsilon^2 V_2 + \ldots \qquad (2.2)$$

$$V_1 = v_1 + a_{1j}q_j + b_{1jk}q_jq_k + c_{1jkl}q_jq_kq_l + d_{1jklm}q_jq_kq_lq_m + \ldots \qquad (2.3)$$

$$V_2 = v_2 + a_{2j}q_j + b_{2jk}q_jq_k + c_{2jkl}q_jq_kq_l + d_{1jklm}q_jq_kq_lq_m + \ldots \qquad (2.4)$$

The universal imperfection magnitude parameter, ε is a measure of the magnitude of deviation in material and structural properties from the perfect structure. In this way, imperfections can be modeled as deviations. In general, any structural or material property F can be modeled as $F(x) = F_0[1 + \varepsilon f(x)]$ with a mean value of F_0 and an imperfection pattern $f(x)$.

When $\varepsilon = 0$, the structure is reduced to the perfect structure. However, the product of the imperfection being considered and the critical imperfection magnitude ε_{cr} must be sufficiently small (<0.35) in order for the power series expansion to converge. Therefore, the "actual structure" (as defined by the imperfection patterns) is never actually encountered in CIM. In short, the approach used by CIM is to set a given load, use imperfection patterns to define the "actual structure," and solve for the smallest ε that causes buckling at the given load. The engineer can then check the true actual structure against the CIM "actual structure" and the critical imperfection magnitude.

Most of the imperfection patterns in this study will be simulated by spectral representation. This concept will be developed briefly at the end of this chapter. The end load eccentricities will be modeled as imperfections described by Gaussian distributions. This will be discussed in detail in Chapter III.

Continuing the development of CIM, *Equation 2.2* can be rewritten in the following more general form:

$$
\begin{aligned}
V = \; & (v_0 + \varepsilon v_1 + \varepsilon^2 v_2 + ...) \\
& + (a_{0j} + \varepsilon a_{1j} + \varepsilon^2 a_{2j} + ...)q_j \\
& + (b_{ojk} + \varepsilon b_{1jk} + \varepsilon^2 b_{2jk} + ...)q_j q_k \\
& + (c_{0jkl} + \varepsilon c_{1jkl} + \varepsilon^2 c_{2jkl} + ...)q_j q_k q_l \\
& + (d_{ojklm} + \varepsilon d_{1jklm} + \varepsilon^2 d_{2jklm} + ...)q_j q_k q_l q_m + ...
\end{aligned}
\tag{2.5}
$$

The equilibrium and stability criteria of the actual structure may be derived from the first and second variations of the potential energy, V. Readers unfamiliar with energy methods and variational principles are referred to Langhaar (1989) and Bazant and Cedolin (1991) for details and mathematical proofs.

11

Although the coefficients $a_{(\cdot)}$, $b_{(\cdot)}$, $c_{(\cdot)}$, and $d_{(\cdot)}$ need not be symmetric, they can always be selected to be symmetric with respect to any permutation of their indices in order to take advantage of the numerical efficiency of CIM. The variational equations, after grouping the coefficients for the appropriate generalized coordinates, are:

$$\Delta V = V(q_j + \delta q_j, q_k + \delta q_k) - V(q_j, q_k) \tag{2.6}$$

$$\begin{aligned} \Delta V = {} & (a_{oj} + \varepsilon a_{1j} + \varepsilon^2 a_{2j} + ...)(\Delta q_j) \\ & + (b_{0jk} + \varepsilon b_{1jk} + \varepsilon^2 b_{2jk} + ...)(\Delta(q_j q_k)) \\ & + (c_{0jkl} + \varepsilon c_{1jkl} + \varepsilon c_{2jkl} + ...)(\Delta(q_j q_k q_l)) \\ & + (d_{0jklm} + \varepsilon d_{1jklm} + \varepsilon^2 d_{2jklm} + ...)(\Delta(q_j q_k q_l q_m)) \end{aligned} \tag{2.7}$$

where

$$\Delta q_j = (q_j + \delta q_j) - q_j = \delta q_j \tag{2.8}$$

$$\begin{aligned} \Delta q_j q_k &= (qj + \delta q_k)(q_k + \delta q_k) - (q_j q_k) \\ &= q_j(\delta q_k) + q_k(\delta q_j) + (\delta q_j)(\delta q_k) \end{aligned} \tag{2.9}$$

$$\begin{aligned} \Delta(q_j q_k q_l) &= [q_j(\delta q_j)][q_k(\delta q_k)][q_l(\delta q_l)] - (q_j q_k q_l) \\ &= q_j q_k(\delta q_l) + q_l q_j(\delta q_k) + q_k q_l(\delta q_j) + q_j(\delta q_k)(\delta q_l) \\ &\quad + q_l(\delta q_j)(\delta q_k) + q_k(\delta q_l)(\delta q_j) + (\delta q_j)(\delta q_k)(\delta q_l) \end{aligned} \tag{2.10}$$

$$\Delta(q_j q_k q_l q_m) = [q_j + (\delta q_j)][q_k + (\delta q_k)][q_l + (\delta q_l)][q_m + (\delta q_m)]$$

$$- (q_j q_k q_l q_m)$$

$$= q_j q_k q_l q_m + q_j q_k q_l (\delta q_m) + q_j q_k q_m (\delta q_l)$$

$$+ q_j q_k (\delta q_l)(\delta q_m) + q_j q_l q_m (\delta q_k) + q_j q_l (\delta q_k)(\delta q_m)$$

$$+ q_j q_m (\delta q_k)(\delta q_l) + q_j (\delta q_k)(\delta q_l)(\delta q_m)$$

$$+ q_k q_l q_m (\delta q_j) + q_k q_l (\delta q_j)(\delta q_m) + q_k q_m (\delta q_j)(\delta q_l) \qquad (2.11)$$

$$+ q_k (\delta q_j)(\delta q_l)(\delta q_m) + q_l q_m (\delta q_j)(\delta q_k)$$

$$+ q_l (\delta q_j)(\delta q_k)(\delta q_m) + q_m (\delta q_j)(\delta q_k)(\delta q_l)$$

$$+ (\delta q_j)(\delta q_k)(\delta q_l)(\delta q_m) - q_j q_k q_l q_m$$

The first and second variational equations for the potential energy of the actual structure may be obtained by combining *Equations 2.6-2.11*:

$$\delta V = \{(a_{0j} + \varepsilon a_{1j} + \varepsilon^2 a_{2j} + \dots)$$

$$+ 2(b_{0jk} + \varepsilon b_{1jk} + \varepsilon^2 b_{2jk} + \dots)q_k$$

$$+ 3(c_{0jkl} + \varepsilon c_{1jkl} + \varepsilon^2 c_{2jkl} + \dots)q_k q_l \qquad (2.12)$$

$$+ 4(d_{0jklm} + \varepsilon d_{1jklm} + \varepsilon^2 d_{2jklm} + \dots)q_k q_l q_m\}(\delta q_j)$$

$$\delta^2 V = \{2(b_{0jk} + \varepsilon b_{1jk} + \varepsilon^2 b_{2jk} + \dots)$$

$$+ 6(c_{0jkl} + \varepsilon c_{1jkl} + \varepsilon^2 c_{2jkl} + \dots)q_l \qquad (2.13)$$

$$+ 12(d_{0jklm} + \varepsilon d_{1jklm} + \varepsilon^2 d_{2jklm} + \dots)q_l q_m\}(\delta q_j)(\delta q_k)$$

Equations 2.12 and 2.13 represent the potential energy expansion of the actual structure. There is a second expansion in CIM which is taken around the pre-buckling equilibrium state q_{0j} of the perfect structure. Then, the pre-buckling equilibrium state q_j of the actual structure are expanded around this point.

$$q_j = q_{0j} + \varepsilon q_{1j} + \varepsilon^2 q_{2j} + \dots \qquad j = 1, 2, \dots, M \qquad (2.14)$$

$$q_j q_k = q_{0jk} + \varepsilon q_{1jk} + \varepsilon^2 q_{2kl} + \dots \qquad (2.15)$$

$$q_j q_k q_l = q_{0jkl} + \varepsilon q_{1jkl} + \varepsilon^2 q_{2jkl} + \dots \qquad (2.16)$$

$$q_j q_k q_l q_m = q_{0jklm} + \varepsilon q_{1jklm} + \varepsilon^2 q_{2jklm} + \dots \qquad (2.17)$$

This expansion is made possible due to the fact that experiments have shown small, smoothly varying imperfections have very little effect on the initial pre-buckling response of a structure. Expansion around the pre-buckling point therefore will introduce only infinitesimal error into the formulation. Substitution of *Equations 2.14-2.17* into *Equations 2.12 and 2.13* establishes the pre-buckling equilibrium path. This is illustrated in *Figure 2.1*. The structure buckles at the bifurcation point which is the lowest point of instability on the path. Mathematically, this is the point where $\delta^2 V$ goes from positive definite to positive semi-definite for the first time.
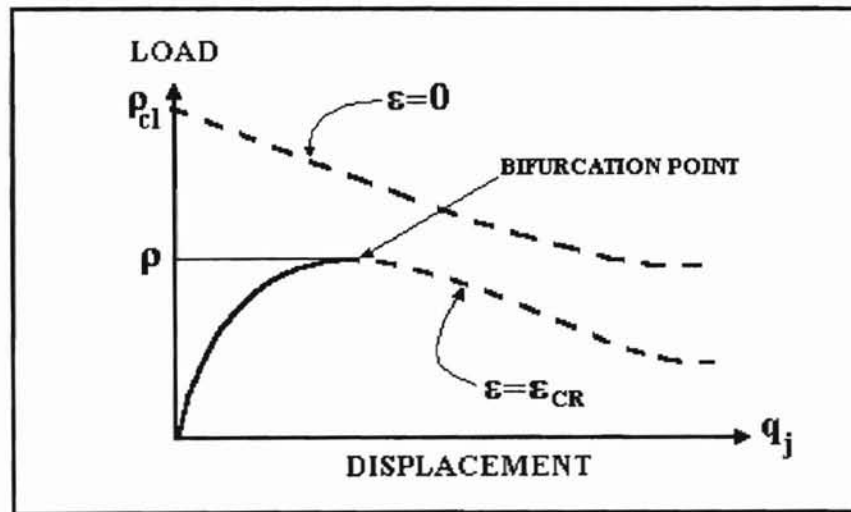
Figure 2.1: Load-Displacement Diagram

The central idea behind the development of CIM is to formulate a generalized eigenvalue problem in terms of ε for a given load ρ. Thus, the smallest ε that provides a

14

non-trivial solution of the eigenvalue problem represents the critical imperfection magnitude, ε_{cr}. Also, physically ε_{cr} represents the bifurcation point.

The numerical efficiency of CIM can be brought into play by the use of incremental coordinates and orthogonal displacement modes. A significant simplification can be made by using generalized coordinates that are measured incrementally from the perfect structure reference state, q_{0j}. That is, $q^*_j = q_j - q_{0j}$. For the beam on elastic foundation that will be considered in this thesis, $q_{0j} = 0$. The previously mentioned coefficients $a_{(\cdot)}$, $b_{(\cdot)}$, $c_{(\cdot)}$, and $d_{(\cdot)}$ are transformed to be symmetric with respect to any permutation of their indices.

The geometric stiffness matrix, b_{0jk} of the perfect structure is always positive definite up to the classical buckling load and for the prebuckling range of imperfection-sensitive structures. Therefore, its inverse always exists. For more efficient numerical calculation, the generalized coordinates are chosen such that b_{0jk} is diagonal. This can be accomplished by the use of Kronecker's delta, δ_{jk} such that $r_{jk}b_{0jk} = \delta_{jk}$. The transformed generalized coordinates now take the form $q_j^* = r_{jl}q_l^{**}$.

The eigenvalue problem can now be simplified by taking the Hermitian form in the new generalized coordinates, q_j^{**}, $j = 1, 2, ..., M$, where M is the number of buckling modes to be considered in the problem. As demonstrated by Palassopoulos (1993), the following condition leads to instability in a structure:

$$(V_{0jk} + \varepsilon V_{1jk} + \varepsilon^2 V_{2jk} + ...)(\delta q_k) = 0 \qquad j = 1, 2, ..., M \qquad (2.18)$$

$$V_{0jk} = 2b_{0jk} \qquad (2.19)$$

$$V_{1jk} = 2b_{1jk} + 6c_{0jkl}q_{1l} \qquad (2.20)$$

$$V_{2jk} = 2b_{jk} + 6c_{0jkl}q_{2l} + 6c_{1jkl}q_{1l} + 12d_{0jklm}q_{1l}q_{1m} \qquad (2.21)$$

15

Substituting *Equations 2.19-2.21* into *Equation 2.18* gives the Hermitian (symmetric) form of the characteristic equation:

$$(\varepsilon\gamma_{1jk} + \varepsilon^2\gamma_{2jk} + ...)(\delta q_k) = (\delta q_j) \tag{2.22}$$

$$\gamma_{1jk} = \frac{1}{\sqrt{b_{0jj}b_{0kk}}}\left[-b_{1jk} + \frac{3c_{0jkl}a_{1l}}{2b_{0ll}}\right] \tag{2.23}$$

$$\gamma_{2jk} = \frac{1}{\sqrt{b_{0jj}b_{0kk}}}\left[-b_{2jk} + \frac{3c_{1jkl}a_{1l}}{2b_{0ll}} + \frac{3c_{0jkl}a_{2l}}{2b_{0ll}} - \frac{3c_{0jkl}b_{1lm}a_{1m}}{2b_{0ll}b_{0mm}}\right.$$

$$\left. + \frac{9c_{0jkl}c_{0lmn}a_{1m}a_{1n}}{8b_{0ll}b_{0mm}b_{0nn}} - \frac{3d_{0jklm}a_{1l}a_{1m}}{2b_{0ll}b_{0mm}}\right] \tag{2.24}$$

Equation 2.22 is the generalized eigenvalue problem. This eigenvalue problem includes both symmetric bifurcation (e.g. beam on elastic foundation, Euler columns, plates, etc.) and asymmetric bifurcation (e.g. thin cylindrical shells). When c_{0jkl} vanishes identically to zero, the generalized eigenvalue problem becomes unstable symmetric, which is the special case corresponding to the symmetric bifurcation buckling of Koiter's Theory. When c_{0jkl} vanishes, *Equations 2.23 and 2.24* can be simplified to :

$$\gamma_{1jk} = \frac{-b_{1jk}}{\sqrt{b_{0jj}b_{0kk}}} \tag{2.25}$$

$$\gamma_{2jk} = \frac{1}{\sqrt{b_{0jj}b_{0kk}}}\left(-b_{2jk} + \frac{3c_{1jkl}a_{1l}}{2b_{0ll}} - \frac{3d_{0jklm}a_{1l}a_{1m}}{2b_{0ll}b_{0mm}}\right) \tag{2.26}$$

The matrix form of the second-order eigenvalue problem, which will be used in this thesis, can be written as shown in *Equation 2.27* with submatrices γ, I, and 0 where "I" is the identity matrix and "0" is the null matrix. The size of the matrix γ is equal to the

order of buckling modes M. Thus, there are M eigenvalues, ε. It is not an overly complicated matter to extend *Equation 2.27* to higher value orders if required.

$$\begin{bmatrix} \gamma_1 & \gamma_2 \\ I & 0 \end{bmatrix} \begin{Bmatrix} \delta q \\ \varepsilon \delta q \end{Bmatrix} = \frac{1}{\varepsilon} \begin{Bmatrix} \delta q \\ \varepsilon \delta q \end{Bmatrix} \qquad (2.27)$$

There are many types of structural imperfections. However, the four main types of imperfections occur in (1) shape, (2) material properties, (3) geometry, and (4) the applied load. Palassopoulos (1993) classified shape imperfections (i.e., imperfections that relate to curvature in the beam) as Type I and all others as Type II.

Eccentricity in the applied load when modeled as an imperfection is of Type I because the resulting end moments induce curvature into the beam. Qualitatively, for the beam on elastic foundation the a_{ij} term is an indication of Type I (shape) imperfections. As will be demonstrated in Chapter III, the a_{1j} term is the only term in the characteristic equation that is affected by the eccentricity imperfections.

Many researchers have modeled imperfections through a deterministic approach. However, the resulting mathematical complexity is often only a source of frustration, serving only to obscure the physics of the problem. However, structural imperfections are actually stochastic in the sense that their specific nature cannot be prescribed. In recent years, advancements in stochastic mechanics and computers have made it possible to simulate imperfections as random variables with some ease.

As with any theory or idea, there are limitations to CIM. One of these is that the quantitative application of CIM requires detailed measurement of the imperfections. Quite likely, it would be an expensive and time consuming task to measure a structure for all small imperfections. Instead, Palassopoulos (1993) suggested a stochastic approach

17

which would combine reliability engineering with CIM to get around this problem. This was the approach used by Yeigh (1995) in his work, and it is the approach that will be used in this thesis.

The three imperfection patterns that will be used in this thesis are (1) bending rigidity e(x), (2) foundation stiffness k(x), and (3) shape h(x). The varying components of bending rigidity and foundation stiffness are normalized by their respective expected values. The shape of the beam is non-dimensionalized by the modified beam length L_P, where $L_P = L/\pi$ = Span Length L divided by π. As it will later become evident, this substitution will enable more efficient numerical solution of the coefficients in the characteristic equation. As it was already mentioned, the eccentricity imperfections η_1 and η_2 will be modeled as single-value random variables.

The imperfection patterns are assumed to be one-dimensional, homogenous, Gaussian random fields. Due to the Central Limit Theorem, the simulated imperfection fields are asymptotically Gaussian as N approaches infinity. Using the cosine series formula [Shinozuka and Deodatis 1991], the spectral representation method has proven to be very computationally efficient. Also, the ensemble average power spectral density function (PSD) approaches the corresponding target function with increasing sample size.

In general, the structural property F(x) varies as a function of the non-dimensional axial coordinate x, since the imperfection pattern it represents is assumed to be a one-dimensional, univariate, (1D-1V) homogeneous, Gaussian stochastic field:

$$F(x) = F_0[1+\varepsilon f(x)] \tag{2.28}$$

Where F_0 is the expected value of F(x), and ε is the perturbation parameter. The function f(x) represents the imperfection pattern which is a 1D-1V, homogeneous, Gaussian

18

stochastic field with a zero mean. F(x) may be written in terms of the cosine series with a

deterministic amplitude A_n, and a random phase angle φ_n.

$$f(x) = \sqrt{2}\sum_{n=1}^{N} A_n \cos(\kappa_n x + \varphi_n) \tag{2.29}$$

$$A_n = \left(G_{ff}(\kappa_n)\Delta\kappa\right)^{\frac{1}{2}} \tag{2.30}$$

$$\kappa_n = n\Delta\kappa = n\frac{\kappa_u}{N} \qquad n = 1, 2, ..., N \tag{2.31}$$

In *Equations 2.29-2.31*, κ is the wave number and κ_u is the fixed upper cut-off wave

number. The value of κ_u is chosen such that above it, the corresponding one-sided power

spectral density $G_{ff}(\kappa)$ is zero or negligibly small. This is done either for mathematical or

physical reasons. The following power spectral density function and corresponding

autocorrelation function are used:

$$G_{fofo}(\kappa_0) = \frac{1}{2}\sigma_{fo}{}^2 b_{fo}{}^3 \kappa_o{}^2 \exp\left[-b_{fo}|\kappa_o|\right] \tag{2.32}$$

$$R_{fofo}(\xi_0) = \sigma_{fo}{}^2 \frac{1 - 3\left(\dfrac{\xi_o}{b_{fo}}\right)^2}{\left[1 + \left(\dfrac{\xi_o}{b_{fo}}\right)^2\right]^3} \tag{2.33}$$

These equations are used primarily because they are general, simple, versatile, and

because they have been shown to give good results in previous work [Yeigh 1995].

The correlation distance, b_{fo}, is chosen to best match the PSD to the expected

degree of fluctuation in the imperfections. For long values of b_{fo}, the PSD more or less

slowly undulates, and its difference in magnitude at two neighboring regions may not be

very significant. For short b_{fo}, the PSD varies sharply and rapidly down the axis of the

beam. The correlation distance corresponding to *Equations 2.32-2.33* used in this study is 1.50. This is a reasonable, average, and realistic choice that will more accurately reflect an actual beam with imperfections. As the correlation distance goes above 1.50, the shape imperfections tend to have less and less effect because of the reduced magnitude of the initial curvature changes [Yeigh 1995]. On the other hand, when b_{fo} is less than 1.50, the PSD becomes sharply "jagged" and the shape imperfections overwhelmingly dominate the buckling of the beam.

A possible extension of this thesis would of course be through the use of different power spectral density functions, appropriate autocorrelation functions, and various correlation distances. The reader is referred to Shinozuka (1987) for more details.

CHAPTER III. *Beam on Elastic Foundation*

The beam on elastic foundation (BEF) with imperfections in initial shape, bending rigidity, foundation stiffness, and eccentric end loads will be considered in this thesis. The addition of eccentric loads into the ensemble of imperfections is an extension of the work completed by Yeigh (1995). He was the first to apply stochastic methods and CIM to study the interactions of various imperfections other than, and including, those of initial shape.

The BEF provides a simple, one-dimensional platform to model other more complicated structures, and is capable of demonstrating varying degrees of imperfection sensitivity [Palassopoulos 1993]. The BEF is a prototypical model which may be extended to higher dimensions such as plates, frames, trusses, and cylindrical shells. Examples of the BEF include, among others: drilled piers, strip footings, pavement, shear wall columns, and even ice sheets floating on water.

The first step in the formulation of any analytical model is, of course, to define the coordinate system that will be used. The coordinate system for this thesis is the standard right-hand system with positive X-axis pointing to the right, positive Y-axis pointing down, and all moments and rotations positive clockwise.

Next, consider a simply supported beam on a linear elastic foundation. See *Figure 3.1*. The axial compressive load is denoted by P, the length is L, the elastic foundation stiffness is K, and the axial coordinate is X. The beam has a lateral displacement W, and bending rigidity EI, and eccentricity of load Z_1 (on the left) and Z_2 (on the right) which are not shown. The beam also has a depth, d_e. The variable d_e does not explicitly enter the potential energy formulation. However, in order to model the distribution of the end eccentricities, the

depth must be physically defined. This can be achieved by relating d_e to L by means of a span-to-depth ratio. For this study, a commonly used engineering span-to-depth ratio of 20 is used.
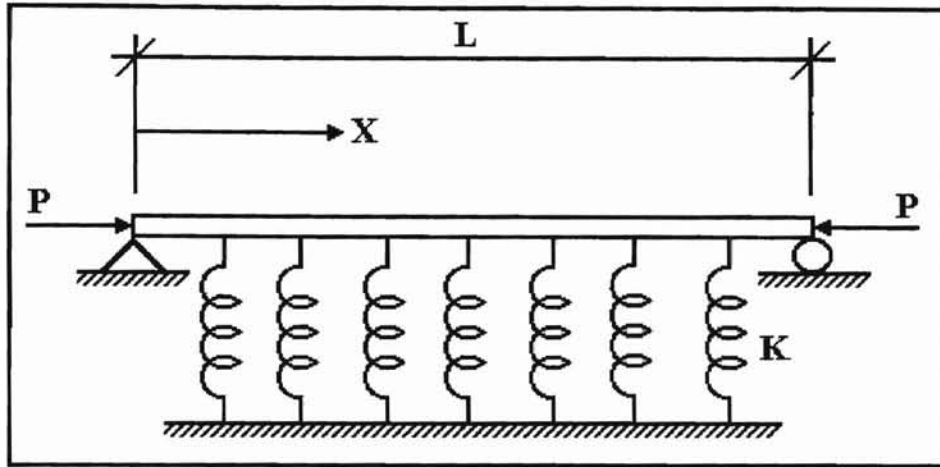
Figure 3.1. Beam on elastic foundation

For generality, the dimensional coordinates will be non-dimensionalized. This will also make the resulting formulation more readily suitable for analytic calculation. For this problem, the most convenient approach to a non-dimensional form is to divide the length variables by the modified span length, $L_P = L / \pi$. Also, if the mean value of the bending rigidity EI is $(EI)_0$, the other variables can be made non-dimensional as well.

$$x = \frac{X}{L_P} = \frac{\pi X}{L} \tag{3.1}$$

$$w = \frac{W}{L_P} = \frac{\pi W}{L} \tag{3.2}$$

$$z_1 = \frac{Z_1}{L_P} = \frac{\pi Z_1}{L} \tag{3.3}$$

$$z_2 = \frac{Z_2}{L_P} = \frac{\pi Z_2}{L} \tag{3.4}$$

$$\varphi = \frac{L_P^4}{(EI)_0}K = \frac{L^4}{\pi^4(EI)_0}K \tag{3.5}$$

$$\rho = \frac{L_P^2}{(EI)_0}P = \frac{L^2}{\pi^2(EI)_0}P \tag{3.6}$$

For completeness, the potential energy of the system that will be derived, V, can also be made non-dimensional at this point.

$$v = \frac{L_P}{(EI)_0}V = \frac{L}{\pi(EI)_0}V \tag{3.7}$$

Next, the imperfections that will be considered are defined in terms of their respective imperfection patterns. In CIM, all imperfections and their combinations can be considered. This thesis will concentrate on imperfections of shape (Type I), bending rigidity (Type II), foundation stiffness (Type II), and eccentricity of load (Type I). Imperfections in shape determine the initial shape (or "crookedness") of the beam along the x-axis. Imperfections in bending rigidity and foundation stiffness determine how Young's Modulus, the moment of inertia, and the elasticity of the foundation vary along the beam, respectively. Imperfections in eccentricity determine how the eccentricity of the applied load vary on the ends of the beam. The various structural and geometric properties that are affected by imperfections may be defined as:

$$EI(x) = (EI)_0[1 + \varepsilon e(x)] \tag{3.8}$$

$$\varphi(x) = \varphi_0[1 + \varepsilon k(x)] \tag{3.9}$$

$$w_0 = \varepsilon h(x) \tag{3.10}$$

$$z_1 = \varepsilon \eta_1 \tag{3.11}$$

$$z_2 = \varepsilon \eta_2 \tag{3.12}$$

$$K(x) = K_0[1 + \varepsilon k(x)] \tag{3.13}$$

$$\varphi_0 = \frac{L_P^4}{(EI)_0} K_0 = \frac{L^4}{\pi^4 (EI)_0} K_0 \tag{3.14}$$

In *Equations 3.8-3.12*, ε is a perturbation parameter that is known in CIM as the universal imperfection magnitude. The functions $e(x)$, $k(x)$, and $h(x)$ are the imperfection patterns (stochastic fields) for the beam to be used on the bending rigidity, foundation stiffness, and initial shape respectively. The terms η_1 and η_2 are independent random variables. For the case of a Gaussian distribution, η is distributed normally with zero mean and standard deviation σ_η.

For physical reasons, the distributions for η are truncated at the top and bottom edges of the beam. The central idea is that the eccentricities are accidental. That is, they are imperfections with a zero mean. Therefore, the loads must at least be on the beam.

There are many distributions one could use to model different situations and intentions. For example, the beta distribution has been suggested as a possible model because it has been shown to fit certain observed phenomena. Also, the uniform distribution could be used for the case of completely unknown eccentricities such as "uniformly" loaded piles, or drilled piers. In these cases, the only information known is that the centroid of the applied load is somewhere on the end of the beam (maintaining the limitation that it must actually be on the beam).

The Gaussian distribution was chosen here because of its widespread application. It can be used without losing any generality. The standard deviation that will be used in the Gaussian distribution is 5% of the beam depth. This value was chosen to more realistically

24

reflect the situation of unintentional eccentricity because any eccentricity that so develops will have a very strong central tendency. The use of other distributions and statistical parameters would certainly be capable of producing a deeper physical insight into the mechanics of eccentric load imperfection buckling and would be an excellent means to extend this thesis.

This thesis is concerned with the inextensional case of the BEF. That is, the beam does not undergo any axial deformation prior to buckling. The x-coordinate is defined to be the line through the gravity center of the beam, and it deflects with the beam. After the beam deflects, the fixed spatial coordinate is designated X^*. See *Figure 3.2.*
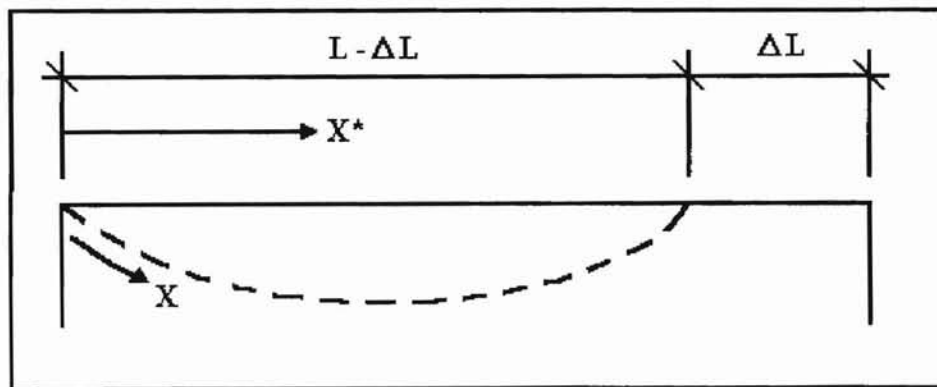

Figure 3.2. Deflected X-coordinate of the beam on elastic foundation

Using the Pythagorean Formula, it can readily be seen that $dX^{*2} = dX^2 + dW^2$. After a small amount of algebraic manipulation, ΔL can be solved:

$$\Delta L = L - \int_0^L \sqrt{1 - W'^2}\, dX \qquad (3.15)$$

It is desired to have positively defined end moments M_1 and M_2 in the formulation of V_M. In order for M_1 to be positive, Z_1 must be negative. The reverse is true for M_2. Here, a positive Z_2 gives a positive M_2. The formulations for the positive-value end moments are:

$$M_1 = -PZ_1 \tag{3.16}$$

$$M_2 = PZ_2 \tag{3.17}$$

The potential energy of the system may now be derived. First, the potential energy of the perfect structure will be formulated. Then, after introducing the appropriate imperfections, the potential energy of the actual structure will be developed. Finally, the non-dimensional form of V will be derived.

There are four contributing components to the potential energy of the BEF: (1) V_B, the strain energy of bending due to change in curvature, (2) V_K, the strain energy of the foundation, (3) V_P, the potential energy of the applied load, and (4) V_M, the potential energy of the moments resulting from the accidental eccentricities. The potential energy of the *perfect* system is:

$$V = V_B + V_K + V_P + V_M \tag{3.18}$$

$$V_B = \tfrac{1}{2} \int_0^L EIW''(X^*)^2 \, dX = \tfrac{1}{2} \int_0^L EI \left(\frac{W''}{\sqrt{1-W'^2}} \right)^2 dX \tag{3.19}$$

$$V_K = \tfrac{1}{2} \int_0^L KW^2 \, dX \tag{3.20}$$

$$V_P = -P\Delta L = -P \left(L - \int_0^L \sqrt{1-W'^2} \, dX \right) \tag{3.21}$$

$$V_M = -M_1\theta_1 - M_2\theta_2 = PZ_1\theta_1 - PZ_2\theta_2 = P[Z_1 W'(0) - Z_2 W'(L)] \tag{3.22}$$

26

Now, introduction of the imperfections from *Equations 3.8-3.12*, and dividing by $\frac{\pi(EI)_0}{L}$ leads to the development of the non-dimensional form of the potential energy for the *actual* structure:

$$v_B = \frac{1}{2} \int_0^\pi (1 + \varepsilon e) \left[\frac{w''}{\sqrt{1 - w'^2}} - \frac{\varepsilon h''}{\sqrt{1 - \varepsilon^2 h'^2}} \right]^2 dx \tag{3.23}$$

$$v_K = \frac{1}{2} \int_0^\pi \varphi_0 (1 + \varepsilon k)(w - \varepsilon h)^2 dx \tag{3.24}$$

$$v_P = -\rho \left(\pi - \int_0^\pi \sqrt{1 - w'^2} \, dx \right) \tag{3.25}$$

$$v_M = \rho \left\{ \varepsilon \eta_1 \left[w'(0) - w'_0(0) \right] - \varepsilon \eta_2 \left[w'(\pi) - w'_0(\pi) \right] \right\} \tag{3.26}$$

The primes represent differentiation with respect to the non-dimensional axial coordinate x.

Now, substitute the Taylor series expansions for $\sqrt{1 - w'^2}$, and $\frac{1}{\sqrt{1 - w'^2}}$, into the potential energy and delete all terms with ε^n, $n \geq 3$, and w^m, $m \geq 5$. This is a feasible simplification. Inspection of *Equations 2.22-2.24* will show that the deleted terms do not affect the solution of the characteristic equation.

$$\sqrt{1 - w'^2} = 1 - \frac{1}{2} w'^2 - \frac{1}{8} w'^4 - \frac{1}{16} w'^6 + O(w'^8) \tag{3.27}$$

$$\frac{1}{\sqrt{1 - w'^2}} = 1 + \frac{1}{2} w'^2 + \frac{3}{8} w'^4 + \frac{5}{8} w'^6 + O(w'^8) \tag{3.28}$$

The potential energy may now be expressed as:

27

$$v_B = \frac{1}{2} \int_0^\pi \left[(h''^2 - 2eh''w'' - eh''w''w'^2)\varepsilon^2 \right.$$

$$+(-2h''w'' - h''w''w'^2 + ew''^2 + ew''^2w'^2)\varepsilon \qquad (3.29)$$

$$\left. +(w''^2 + w''^2w'^2) \right] dx$$

$$v_K = \frac{1}{2} \int_0^\pi \left[\left(\varphi_0 h^2 - 2\varphi_0 khw \right)\varepsilon^2 + \left(-2\varphi_0 hw + k\varphi_0 w^2 \right)\varepsilon + \left(\varphi_0 w^2 \right) \right] dx \qquad (3.30)$$

$$v_P = -\rho\pi + \rho \int_0^\pi \left(1 - \frac{1}{2}w'^2 - \frac{1}{8}w'^4 \right) dx$$

$$v_M = \rho\eta_1 w'(0)\varepsilon - \rho\eta_2 w'(\pi)\varepsilon - \rho\eta_1 h'(0)\varepsilon^2 + \rho\eta_2 h'(\pi)\varepsilon^2 \qquad (3.31)$$

In order to prepare the potential energy equation for the appropriate substitutions into the characteristic equation of the eigenvalue problem, all terms containing ε^a and w^b are collected into $v_{a,b}$ equations.

$$v_{0,0} = 0 \qquad (3.32)$$

$$v_{0,1} = 0 \qquad (3.33)$$

$$v_{0,2} = \int_0^\pi \left(\frac{1}{2}w''^2 + \frac{1}{2}\varphi_0 w^2 - \frac{1}{2}\rho w'^2 \right) dx \qquad (3.34)$$

$$v_{0,3} = 0 \qquad (3.35)$$

$$v_{0,4} = \int_0^\pi \left(\frac{1}{2}w''^2 w'^2 - \frac{1}{8}\rho w'^4 \right) dx \qquad (3.36)$$

$$v_{1,0} = 0 \qquad (3.37)$$

$$v_{1,1} = \varepsilon \int_0^\pi (-h''w'' - \varphi_0 hw) dx + \varepsilon\rho\eta_1 w'(0) - \varepsilon\rho\eta_2 w'(\pi) \qquad (3.38)$$

28

$$v_{1,2} = \varepsilon \int_0^\pi \left(\frac{1}{2} ew''^2 + \frac{1}{2} k\varphi_0 w^2 \right) dx \tag{3.39}$$

$$v_{1,3} = \varepsilon \int_0^\pi \left(-\frac{1}{2} h''w''w'^2 \right) dx \tag{3.40}$$

$$v_{1,4} = \varepsilon \int_0^\pi \left(\frac{1}{2} ew''^2 w'^2 \right) dx \tag{3.41}$$

$$v_{2,0} = \varepsilon^2 \int_0^\pi \left(\frac{1}{2} h''^2 + \frac{1}{2} \varphi_0 h^2 \right) dx - \varepsilon^2 \rho\eta_1 h'(0) + \varepsilon^2 \rho\eta_2 h'(\pi) \tag{3.42}$$

$$v_{2,1} = \varepsilon^2 \int_0^\pi \left(-eh''w'' - \varphi_0 khw \right) dx \tag{3.43}$$

$$v_{2,2} = 0 \tag{3.44}$$

$$v_{2,3} = \varepsilon^2 \int_0^\pi \left(-\frac{1}{2} eh''w''w'^2 \right) dx \tag{3.45}$$

$$v_{2,4} = 0 \tag{3.46}$$

Equation 3.37 verifies the original hypothesis that the beam on elastic foundation formulation is a symmetric bifurcation model. The BEF is also an unstable bifurcation and imperfection sensitive model [Bazant and Cedolin 1991]. Also, as it was mentioned in Chapter II, when c_{0jk} vanishes identically to zero, the generalized eigenvalue problem is unstable symmetrically.

Before proceeding with the development of the coefficients in the characteristic equation, the spectral representations for $e(x)$, $k(x)$, and $h(x)$ must be developed and substituted into *Equations 3.32-3.46*.

29

$$e(x) = \sum_{j=1}^{N} e_j \cos(\kappa_j^e x + \Phi_j^e)$$ (3.47)

$$k(x) = \sum_{j=1}^{N} k_j \cos(\kappa_j^k x + \Phi_j^k)$$ (3.48)

Unfortunately, a direct representation for $h(x)$ similar to *Equations 3.47 and 3.48* is not possible. The cosine series will not work because the forced end conditions require zero end displacements. However, Yeigh (1995) developed a route around this problem. In effect, his method was to first generate the shape imperfection field using the spectral representation method, and then rotating and translating the field to meet the required boundary conditions. This fitting procedure is described as follows:

$$h^*(x) = \left[\sqrt{2} \sum_{i=1}^{N} h_i \cos(\kappa_j^h x + \Phi_j^h) \right] - cx + h_0$$ (3.49)

and, realizing that $h^*(0) = h^*(\pi) = 0$,

$$h^*(x) = \sum_{j=1}^{N} h_j^* \sin(jx)$$ (3.50)

$$c = \frac{h(\pi) - h(0)}{\pi}$$ (3.51)

$$h_j^* = \frac{2}{\pi} \left[-\int_0^\pi cx \sin(jx)dx - \int_0^\pi h(0) \sin(jx)dx \right.$$

$$\left. + \int_0^\pi \sqrt{2} \sum_{i=1}^{N} h_i \cos(\kappa_j^h x + \Phi_j^h) \sin(jx)dx \right]$$ (3.52)

Finally, the coefficients of the eigenvalue problem $a_{(\cdot)}$, $b_{(\cdot)}$, $c_{(\cdot)}$, and $d_{(\cdot)}$ can be solved from *Equations 3.34-3.48*:

$$b_{0jk} = \frac{\pi}{4}\left(j^4 - \rho j + \varphi_0\right) \tag{3.53}$$

$$d_{0jklm} = -\frac{1}{8}\rho jklm Y_{1jklm} + \frac{1}{12}jklm\left(jkY_{2jklm} + jmY_{2jmkl}\right.$$

$$\left. + klY_{2kljm} + kmY_{2kmjl} + lmY_{2lmjk}\right) \tag{3.54}$$

$$a_{1j} = -\frac{\pi}{2}\left(j^4 + \varphi_0\right)h_j^* + \rho j\left(\eta_1 - \eta_2(-1)^j\right) \tag{3.55}$$

$$b_{1jk} = \frac{\sqrt{2}}{2}\sum_{l=1}^{N}\varphi_0 k_l\left\{\cos\left(\Phi_l^k\right)Y_{3jk\kappa_l^k} - \sin\left(\Phi_l^k\right)Y_{4jk\kappa_l^k}\right\}$$

$$+ j^2 k^2 e_l\left\{\cos(\Phi_l^e)Y_{3jk\kappa_l^e} - \sin(\Phi_l^e)Y_{4jk\kappa_l^e}\right\} \tag{3.56}$$

$$c_{1jkl} = -\frac{\pi}{48}\sum_{m=1}^{N}h_m^* m^2 jkl\left\{jY_{2mjkl} + kY_{mklj} + lY_{2mljk}\right\} \tag{3.57}$$

where:

$$Y_{1jklm} = \int_0^{\pi}\cos(jx)\cos(kx)\cos(lx)\cos(mx)dx$$

$$= \frac{1}{8}\left[\frac{\sin(j-k+l+m)\pi}{j-k+l+m} + \frac{\sin(j-k+l-m)\pi}{j-k+l-m}\right.$$

$$+ \frac{\sin(j-k-l+m)\pi}{j-k-l+m} + \frac{\sin(j-k-l-m)\pi}{j-k-l-m}$$

$$+ \frac{\sin(j+k+l+m)\pi}{j+k+l+m} + \frac{\sin(j+k+l-m)\pi}{j+k+l-m} \tag{3.58}$$

$$\left. + \frac{\sin(j+k-l+m)\pi}{j+k-l+m} + \frac{\sin(j+k-l-m)\pi}{j+k-l-m}\right]$$

31

$$Y_{2jklm} = \int_0^\pi \sin(jx)\sin(kx)\cos(lx)\cos(mx)dx$$

$$= \frac{1}{8}\left[\frac{\sin(j-k+l+m)\pi}{j-k+l+m} + \frac{\sin(j-k+l-m)\pi}{j-k+l-m}\right.$$

$$+ \frac{\sin(j-k-l+m)\pi}{j-k-l+m} + \frac{\sin(j-k-l-m)\pi}{j-k-l-m}$$

$$- \frac{\sin(j+k+l+m)\pi}{j+k+l+m} - \frac{\sin(j+k+l-m)\pi}{j+k+l-m} \qquad (3.59)$$

$$\left. - \frac{\sin(j+k-l+m)\pi}{j+k-l+m} - \frac{\sin(j+k-l-m)\pi}{j+k-l-m}\right]$$

$$Y_{3jkl} = \int_0^\pi \sin(jx)\sin(kx)\cos(lx)dx$$

$$= \frac{1}{4}\left[\frac{\sin(j-k-l)\pi}{j-k-l} + \frac{\sin(j+k+l)\pi}{j+k+l}\right. \qquad (3.60)$$

$$\left. \frac{\sin(j+k-l)\pi}{j+k-l} - \frac{\sin(j+k+l)\pi}{j+k+l}\right]$$

$$Y_{4jkl} = \int_0^\pi \sin(jx)\sin(kx)\sin(lx)dx$$

$$= \frac{1}{4}\left[\frac{\cos(j-k-l)\pi}{j-k-l} - \frac{1}{j-k-l} - \frac{\cos(j-k+l)\pi}{j-k+l} - \frac{1}{j-k+l}\right. \qquad (3.61)$$

$$\left. - \frac{\cos(j+k-l)\pi}{j+k-l} - \frac{1}{j+k-l} - \frac{\cos(j+k+l)\pi}{j+k+l} - \frac{1}{j+k+1}\right]$$

The integrals in *Equations 3.58-3.61* are closed form. The indefinite forms that may

appear in *Equations 3.58-3.61* all become $\lim\limits_{\alpha \to 0} \dfrac{\sin \pi\alpha}{\alpha} = \pi$ or $\lim\limits_{\alpha \to 0} \dfrac{\cos \pi\alpha}{\alpha} = 0$. Having

32

such easily calculated integrals is the primary benefit of non-dimensionalizing the variables. This is a simple but significant improvement in the numerical efficiency of the model because time can be spent chiefly on solving the eigenvalue problem instead of having to numerically integrate the integrals as well.

The formulation is complete, and the coefficients to the characteristic equation are defined. Chapter IV will present the methods and results of the numerical solution.

CHAPTER IV. *Numerical Results*

Solving the eigenvalue problems can be a very complicated, time consuming affair. This is especially true when the order of the characteristic equation is quadratic and higher. In this thesis, the numerical solutions were obtained with a modified version of the program BEF4, written by Professor Bjong Yeigh of Oklahoma State University. The major modifications to the program were made in the computation of the a_{1j} term, and by calling in the eccentric terms η_1 and η_2 from an outside, independently-generated source file. BEF4 is a *FORTRAN* driver containing several subroutines for stochastic CIM, merged with an eigenvalue solver. The eigenvalue solver is the Linear Algebra PACKage (LAPACK) which is available on the public domain.

For the correlation distances of the stochastic fields used in this thesis, previous work [Yeigh 1995] indicates that 16 buckling modes are adequate to provide sufficiently precise eigenvalues. In fact, for these correlation distances, the use of as many as 128 buckling modes refine the precision over the 16-mode case by no more than 1%.

The procedure for the operation of BEF4 is to first edit the input text files ETA.DAT and TIMBER.DAT. For this study, ETA.DAT was generated by the program ETAX. This program generates 2 sets of independent, normally distributed values by means of the Box-Muller transformation [Press et.al. 1989] of univariate random numbers. The file TIMBER.DAT contains the following values:

1. *The order of the imperfections in the problem.* This value directs BEF4 to proceed with the most efficient solution to the problem by computing only what is necessary (such as γ_1 in the case of Type II imperfections only). The possible values and the

corresponding imperfections that are present are: 1 = h only; 21 = e only; 22 = k only; 23 = e and k; 31 = e and h; 32 = k and h; 33 = e and k and h; e, k , and h imply imperfections in bending rigidity, foundation stiffness, and shape imperfections, respectively. Shape imperfections include accidental eccentric applied loads and initial shape.

2. *The sample size.* In order for the convergence of the dominant eigenvalue to occur, enough samples have to be taken. For the BEF being considered, convergence is essentially complete around 10 to 15 samples. Fifty samples are therefore deemed adequate. One hundred samples were taken to distinguish approximately half of each sample size into pairs of η_1 and η_2 that were alike in sign, with the other half being unalike in sign. Depending on the signs of the η_1 and η_2 pairs, the sense of the moments at the end of the beam due to the eccentric loads could be in the same direction or in the opposite direction. Clearly, these two conditions are different load cases. When the sense of the moments are not the same, the moments tend to force the beam toward single curvature (i.e., Mode I). When they are the same, the beam is directed toward double curvature (i.e., Mode II). Therefore, it was prudent to take enough samples to afford the opportunity to discriminate between the two cases and compare the results. For the sake of brevity in the remainder of this chapter, the case of the ηs having the same sign will be designated η_{SAME}, and the converse will be designated η_{OPP}.

3. *The size of the imperfection modes.* For the power spectral density function and correlation distance used in this thesis, previous work [Yeigh 1995] has shown that

128 imperfection modes are sufficient to adequately capture the shape of the imperfections being considered.

4. *The size of the buckling modes.* As discussed above, this value is set at 16.

5. *The standard deviation of the bending rigidity.* The standard deviation for all imperfection patterns e, k, h* used in this study is 0.05. It is possible to enter these values independently in order to enable the study of mixed imperfections with different standard deviations.

6. *The correlation distance for bending rigidity.* The correlation distance used for all imperfection patterns e, k, and h* in this study is 1.5.

7. *The upper cut-off wave number for bending rigidity.* The upper cut-off wave number used for all imperfection patterns e, k, and h* in this study is 7.447.

8. *A seed value to generate random phase angles for bending rigidity.*

9. *The standard deviation of the foundation stiffness.*

10. *The correlation distance for foundation stiffness.*

11. *The upper cut-off wave number for foundation stiffness.*

12. *A seed value to generate random phase angles for foundation stiffness.*

13. *The standard deviation of the initial shape.*

14. *The correlation distance for initial shape.*

15. *The upper cut-off wave number for initial shape.*

16. *A seed value to generate random phase angles for foundation stiffness.*

17. *The tolerance of the eigenvalue solution.* The tolerance for this study is 0.001.

18. *Soil stiffness parameter.* The nondimensionless soil stiffness parameter used in this study is 225. This value was chosen primarily to afford direct comparison with the results of previous work [Yeigh 1995].

19. *The level of the applied load, ρ below the classical level, ρ_{cl}.* For the BEF, the classical load is the minimum value of $\left(j^2 + \dfrac{\varphi}{j} \right)$ where $j = 1, 2, 3, ..., M$. The value of j is the dominant buckling mode. With $\varphi = 225$, the classical load is therefore 30.0625. The following applied loads were considered: 99%, 97%, 95%, 90%, 85%, 80%, and 75% of the classical load. The dominant buckling mode for this value of φ is the fourth.

The following ensemble of imperfections and imperfection combinations were considered: η alone; $\eta + e$; $\eta + k$; $\eta + h^*$; $\eta + e + k$; $\eta + e + h^*$; $\eta + k + h^*$; and $\eta + e + k + h^*$. As a final step, the η_{SAME} and η_{OPP} cases are separated and compared.

After the two input data text files have been generated and edited, the program BEF4 can be initiated. The operating procedure of BEF4 is as follows:

1. *The equilibrium state q_{oj} is computed.*

2. *The individual or mixed imperfection pattern(s), $e^{(i)}(x)$, $k^{(i)}(x)$, and $h^{*(i)}(x)$ are simulated for each sample $i = 1, 2, 3, ..., N$.*

3. *$h^{(i)}(x)$ is transformed into $h^{*(i)}(x)$.*

4. *The geometric stiffness matrix b_{0ij} is computed.*

5. *b_{0ij} is diagonalized.*

6. *The coefficients $a_{(\cdot)}$, $b_{(\cdot)}$, $c_{(\cdot)}$, and $d_{(\cdot)}$ are computed.*

7. *The coefficient matrix γ is computed.*

8. *The eigenvalue problem is solved.*

9. ε_{RMS} *is solved.*

The solution of the eigenvalue problem for the ith sample imperfection pattern yields the critical imperfection magnitude. For each imperfection parameter, the root mean square (rms) magnitude was then combined with the critical imperfection magnitude, $\varepsilon_{cr}^{(i)}$ according to *Equations 4.1-4.4* to yield the rms imperfection magnitudes, $\varepsilon_{RMS}^{(i)\eta}$, $\varepsilon_{RMS}^{(i)e}$, $\varepsilon_{RMS}^{(i)k}$, and $\varepsilon_{RMS}^{(i)h^*}$:

$$\varepsilon_{RMS}^{(i)\eta} = \varepsilon_{cr}^{(i)} \sqrt{\frac{(\eta_1^{(i)})^2 + (\eta_2^{(i)})^2}{2}} \tag{4.1}$$

$$\varepsilon_{RMS}^{(i)e} = \varepsilon_{cr}^{(i)} \sqrt{\frac{1}{\pi} \int_0^\pi [e^{(i)}(x)]^2 \, dx} \tag{4.2}$$

$$\varepsilon_{RMS}^{(i)k} = \varepsilon_{cr}^{(i)} \sqrt{\frac{1}{\pi} \int_0^\pi [k^{(i)}(x)]^2 \, dx} \tag{4.3}$$

$$\varepsilon_{RMS}^{(i)h^*} = \varepsilon_{cr}^{(i)} \sqrt{\frac{1}{\pi} \int_0^\pi [h^{*(i)}(x)]^2 \, dx} \tag{4.4}$$

Finally, the rms imperfection magnitudes are averaged over the sample size and the results tabulated. These tables can be found in the Appendix.

On average, the scatter in the $\overline{\varepsilon}_{RMS}^{(i)A}$ (where A implies η, e, k, and h^*) was reasonably small with a coefficient of variation on the order of approximately 10%. This is small enough to justify its use as an engineering measure of imperfections. *Figure 4.1* illustrates an example of the convergence of ε_{RMS} over the sample size to the mean value, and *Figure 4.2* is the histogram.
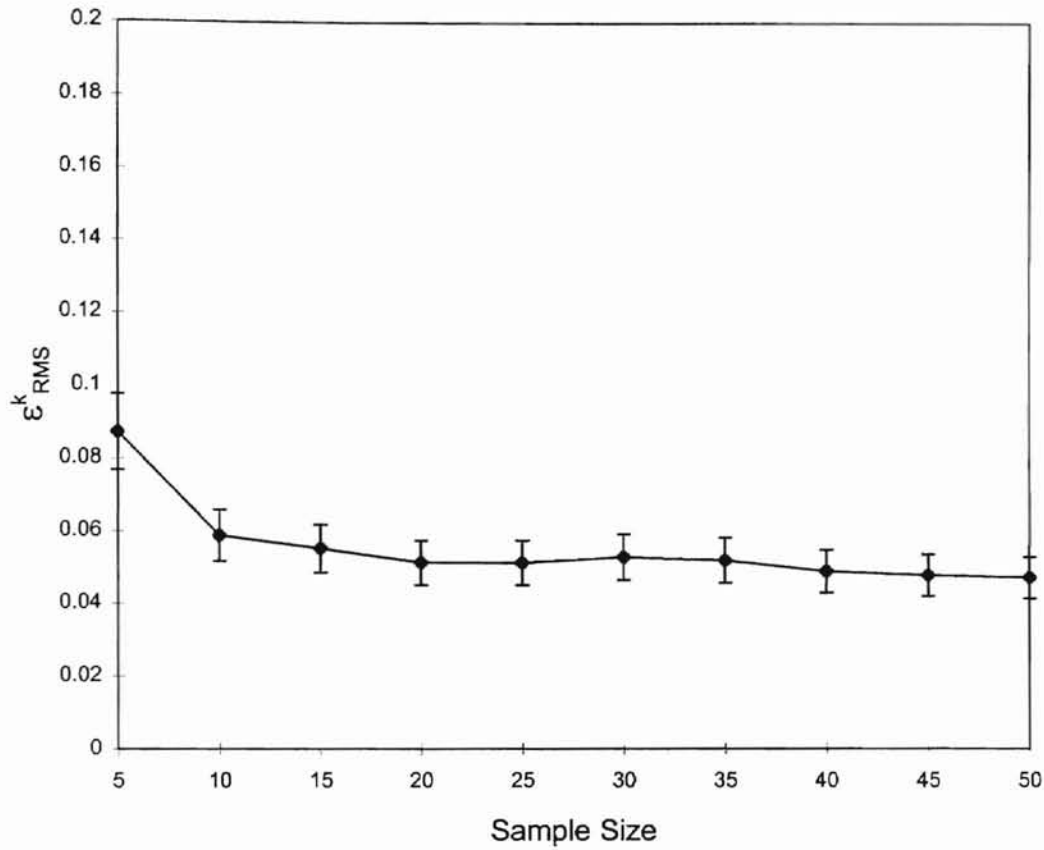
38

Figure 4.1: Convergenge of mean $\varepsilon^k{}_{RMS}$

Foundation stiffness, $\varphi_o = 225$ Sample size ≈ 50

Eccentricity standard deviation, $\sigma_\eta = 0.05$

All other imperfections: $\kappa_{u_o} = 7.449$, $b_{f_o} = 1.50$, $\sigma_{f_o} = 0.05$

Power spectral density function: $G_{f_o f_o}(\kappa_o) = \frac{1}{2}\sigma_{f_o}^2 \, b_{f_o}^3 \kappa_o^2 \exp\left[-b_{f_o}|\kappa_o|\right]$

39

Figure 4.2: Histogram of ε_{RMS}

Foundation stiffness, $\varphi_o = 225$ Sample size ≈ 50

Eccentricity standard deviation, $\sigma_\eta = 0.05$

All other imperfections: $\kappa_{u_o} = 7.449$, $b_{f_o} = 1.50$, $\sigma_{f_o} = 0.05$

Power spectral density function: $G_{f_o f_o}(\kappa_o) = \frac{1}{2} \sigma_{f_o}^2 b_{f_o}^3 \kappa_o^2 \exp\left[-b_{f_o}|\kappa_o|\right]$
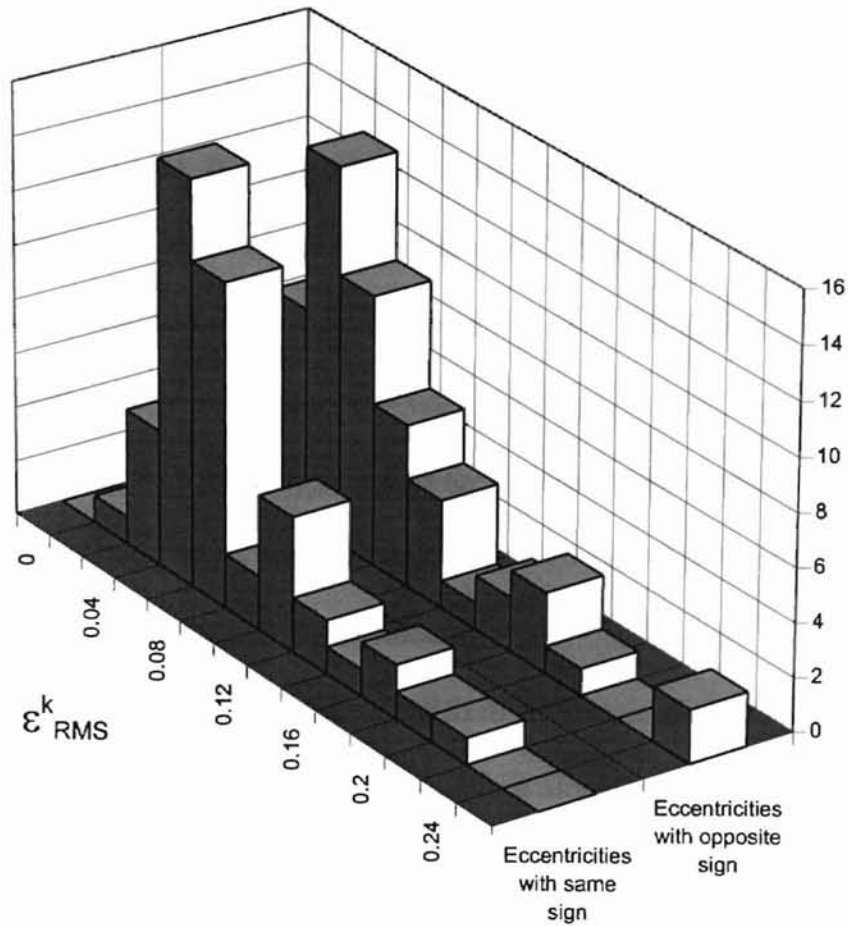
In the figures that follow (*Figures 4.3-4.14*), all axes are dimensionless. The vertical axis indicates the dimensionless normalized load ratio, which is the non-dimensional applied load, ρ divided by the non-dimensional classical load, ρ_{cl}. As previously mentioned, these values range between 0.75 and 0.99. The horizontal axis represents the appropriate ε_{RMS} being considered. In all of the figures, the η_{SAME} case is shown first and the η_{OPP} case is shown second.

In *Figures 4.3 and 4.4,* the ε_{RMS} values for e alone, k alone, and h alone are shown as dotted lines. These values were taken from Yeigh (1995). They are included for reference and were not computed in this research.

Three results are immediately apparent from an examination of the plots. *Figures 4.3 and 4.4* show the direct comparison of ε_{RMS} for η alone, e alone, k alone, and h alone. The first and most important observation is that the eccentricity in the applied loads is an even more dominant imperfection than that of initial shape. It was expected that eccentricity would have a similar effect upon the BEF as does initial shape since it is also a Type I imperfection. The reason eccentricity is dominant in this case is at least in part due to the correlation distance that was used. An average, expected correlation distance was used in this study, which may not always be the case in all situations. Shape imperfections become more and more dominant as the correlation distance decreases [Yeigh 1995]. Therefore, the shape imperfections are not being modeled here in a way that maximizes their dominating effects. On the other hand, the effects on eccentricity imperfection sensitivity will be most pronounced when it is modeled as a random variable, as it is in this case. Thus, the model used in this study maximizes the dominance of the eccentricity imperfection; while holding the dominance of shape

imperfections back to an average. This result is possibly not too surprising given the examples to be learned from engineering experience. Engineers intuitively "know" this already. They know that a slightly dented column is not as dangerous as one with an unintended eccentric load applied to it.

The second result is, of course, that eccentricity is indeed a Type I (shape) imperfection. The ε_{RMS} curves for η are similar in shape, orientation (i.e., concave up), and location as those for h. This result was expected, given that the entry point of the ηs into the characteristic equation was in the a_{1j} term. Again, the engineers already "knew" this. Their experiences have shown that the two cases are somehow related. It will be remembered from Chapter I that the secant formula is often used to model the stress in a column with shape imperfections. That is, the shape imperfections in the column are accounted for as eccentric loads !

The third result, which is perhaps more surprising to intuition than the first, is that there is very little, if any, differences in ε_{RMS} between the η_{SAME} and η_{OPP} cases. This observation is supported somewhat consistently by all of the plots. Intuition would lead one to expect that the η_{SAME} case would always be more detrimental than the η_{OPP} case since it would force the beam to tend toward Mode I buckling. However, this counter-intuitive phenomenon can be explained by realizing that the *perfect* BEF with the prescribed foundation parameter $\varphi = 225$, has the fourth mode as its most dominant mode. That is, the end rotations will have the same direction. Given this, the η_{SAME} case produces one moment that acts in the same direction as one end rotation, while the other moment acts in the opposite direction of its respective end rotation. Therefore, this

behavior may actually be forcing the beam to tend to a higher mode of buckling, not a lower one.

There are actually some small differences in the various plots between the η_{SAME} and η_{OPP} cases, but these variations are quite small. The end result is that it appears to matter little what the signs are on η_1 and η_2 for this BEF. The only item of any tangible consequence is their absolute magnitudes.

In *Figures 4.7-4.10*, the ε_{RMS} plots of η and h are shown for the case when both imperfections are present. Due to the very fine scale of the graphs, the variations in the plots (i.e., their "randomness") are magnified to the extent that they actually become visually obvious. The lines, which have a clearly general direction and tendency, cross one another at various points.

Further study of *Figures 4.7-4.10* show, in the case of ε_{RMS} for η there is a remarkable twentyfold increase in sensitivity when shape imperfections are present. In the case of h, when eccentric loads are present, the sensitivity is increased even more, by about 50 times. It is also obvious from these plots that any detrimental effects from the addition of e and k imperfections are so minor as to be almost inconsequential in the face of the overwhelming dominance of the two Type I imperfections working in conjunction.
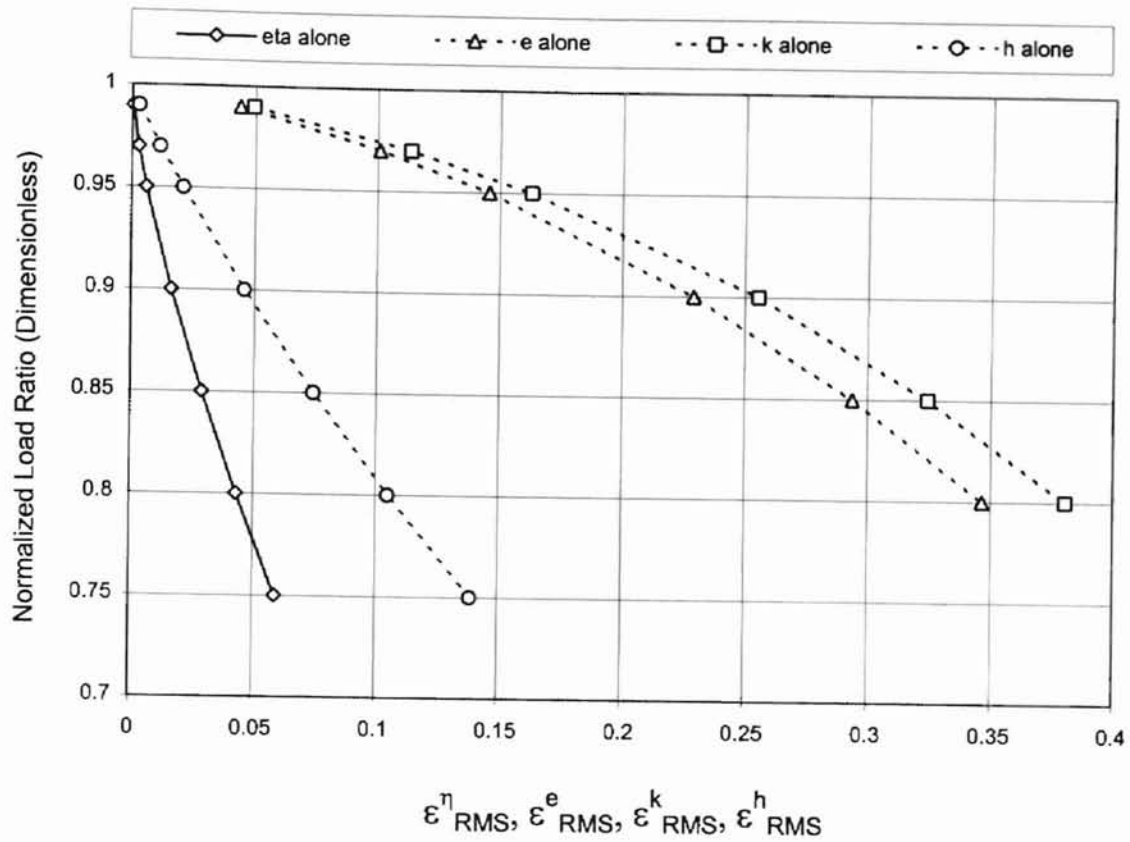
Figure 4.3: Direct comparison of
η_{SAME}, e, k, and h

Foundation stiffness, $\varphi_o = 225$ Sample size ≈ 50

Eccentricity standard deviation, $\sigma_\eta = 0.05$

All other imperfections: $\kappa_{u_o} = 7.449$, $b_{f_o} = 1.50$, $\sigma_{f_o} = 0.05$

Power spectral density function: $G_{f_o f_o}(\kappa_o) = \frac{1}{2}\sigma_{f_o}^2 b_{f_o}^3 \kappa_o^2 \exp\left[-b_{f_o}|\kappa_o|\right]$
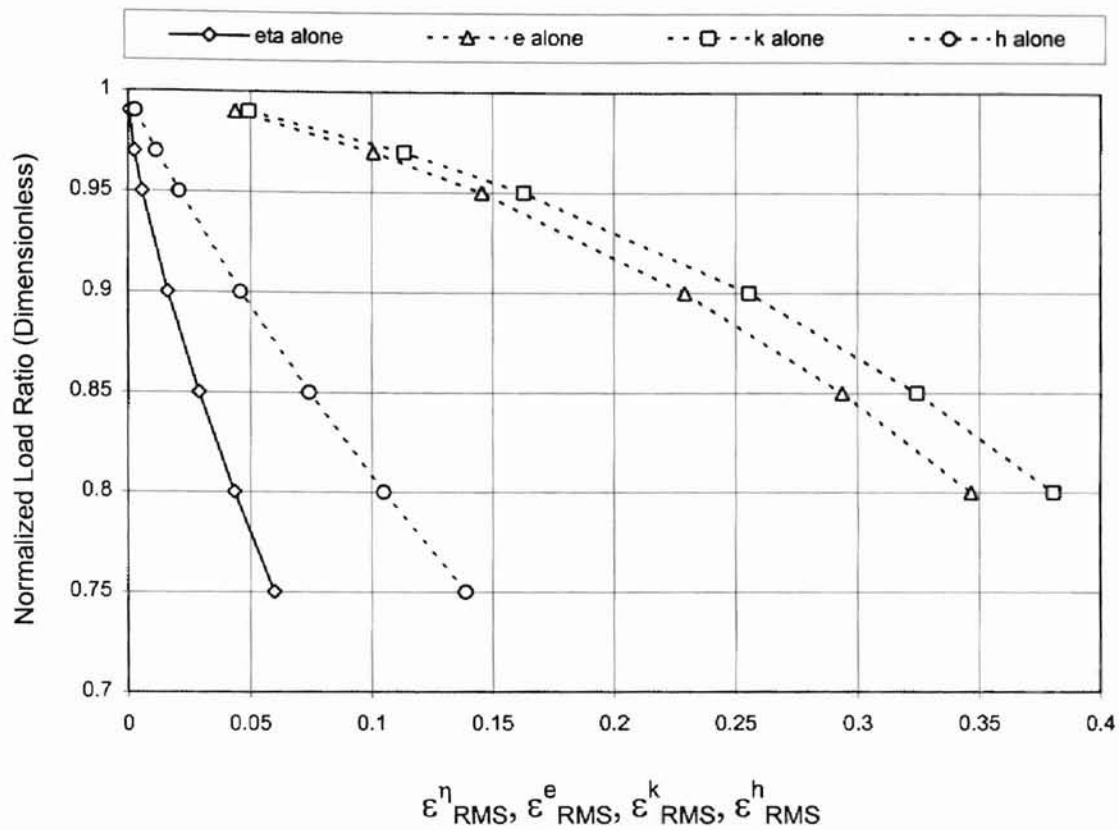
Figure 4.4: Direct comparison of
η_{OPP}, *e, k, and h*

Foundation stiffness, $\varphi_o = 225$ Sample size ≈ 50

Eccentricity standard deviation, $\sigma_\eta = 0.05$

All other imperfections: $\kappa_{u_o} = 7.449$, $b_{f_o} = 1.50$, $\sigma_{f_o} = 0.05$

Power spectral density function: $G_{f_o f_o}(\kappa_o) = \dfrac{1}{2}\sigma_{f_o}^2 b_{f_o}^3 \kappa_o^2 \exp\left[-b_{f_o}|\kappa_o|\right]$
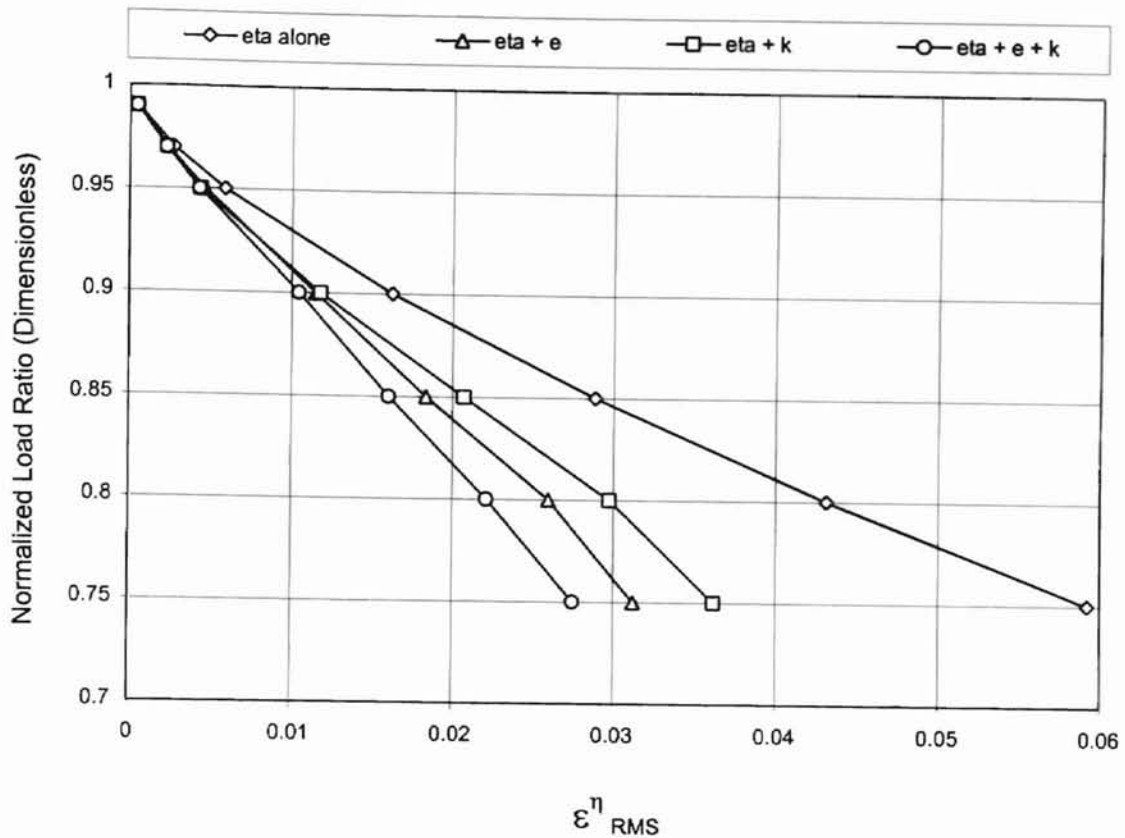
45

Figure 4.5: η_{SAME}

Effects on eccentricity ε^{η}_{RMS}

Foundation stiffness, $\varphi_o = 225$ Sample size ≈ 50

Eccentricity standard deviation, $\sigma_{\eta} = 0.05$

All other imperfections: $\kappa_{u_o} = 7.449$, $b_{f_o} = 1.50$, $\sigma_{f_o} = 0.05$

Power spectral density function: $G_{f_o f_o}(\kappa_o) = \frac{1}{2}\sigma_{f_o}^2 b_{f_o}^3 \kappa_o^2 \exp\left[-b_{f_o}|\kappa_o|\right]$
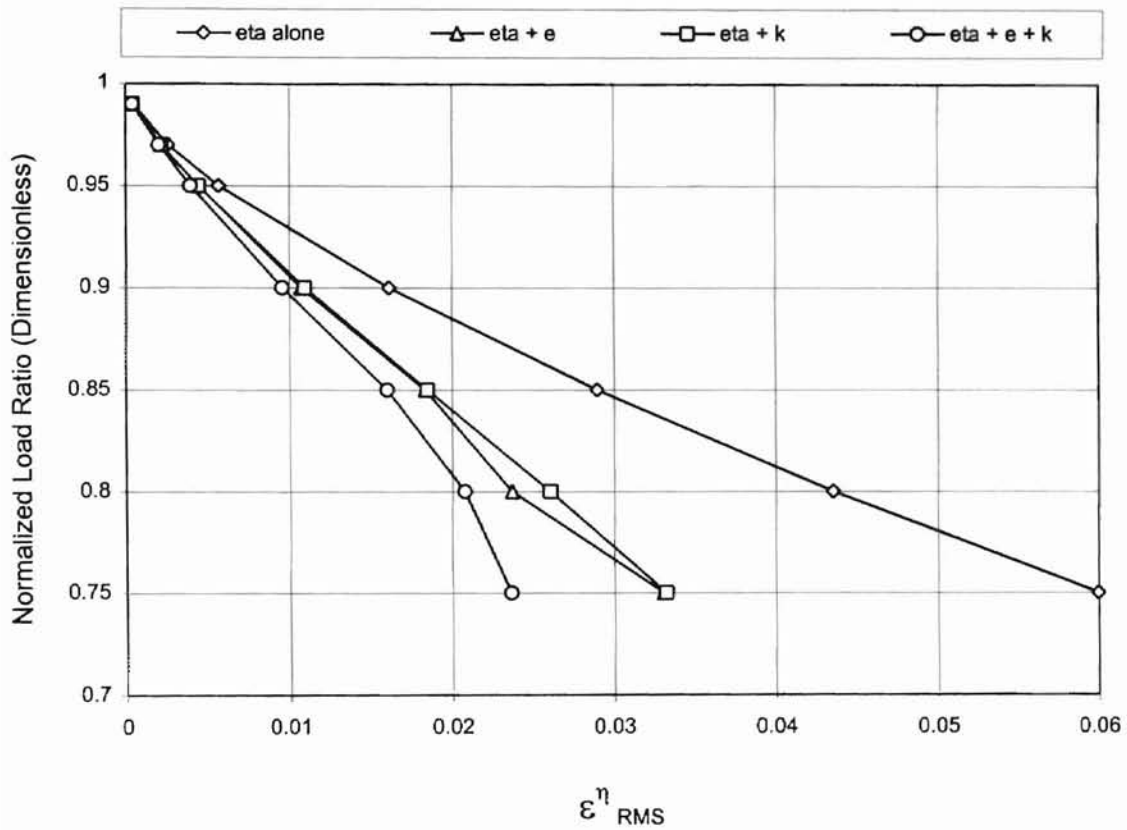
Figure 4.6: η_{OPP}

Effects on eccentricity $\varepsilon^{\eta}{}_{RMS}$

Foundation stiffness, $\varphi_o = 225$ Sample size ≈ 50

Eccentricity standard deviation, $\sigma_{\eta} = 0.05$

All other imperfections: $\kappa_{u_o} = 7.449$, $b_{f_o} = 1.50$, $\sigma_{f_o} = 0.05$

Power spectral density function: $G_{f_o f_o}(\kappa_o) = \frac{1}{2}\sigma_{f_o}^2 b_{f_o}^3 \kappa_o^2 \exp\left[-b_{f_o}|\kappa_o|\right]$
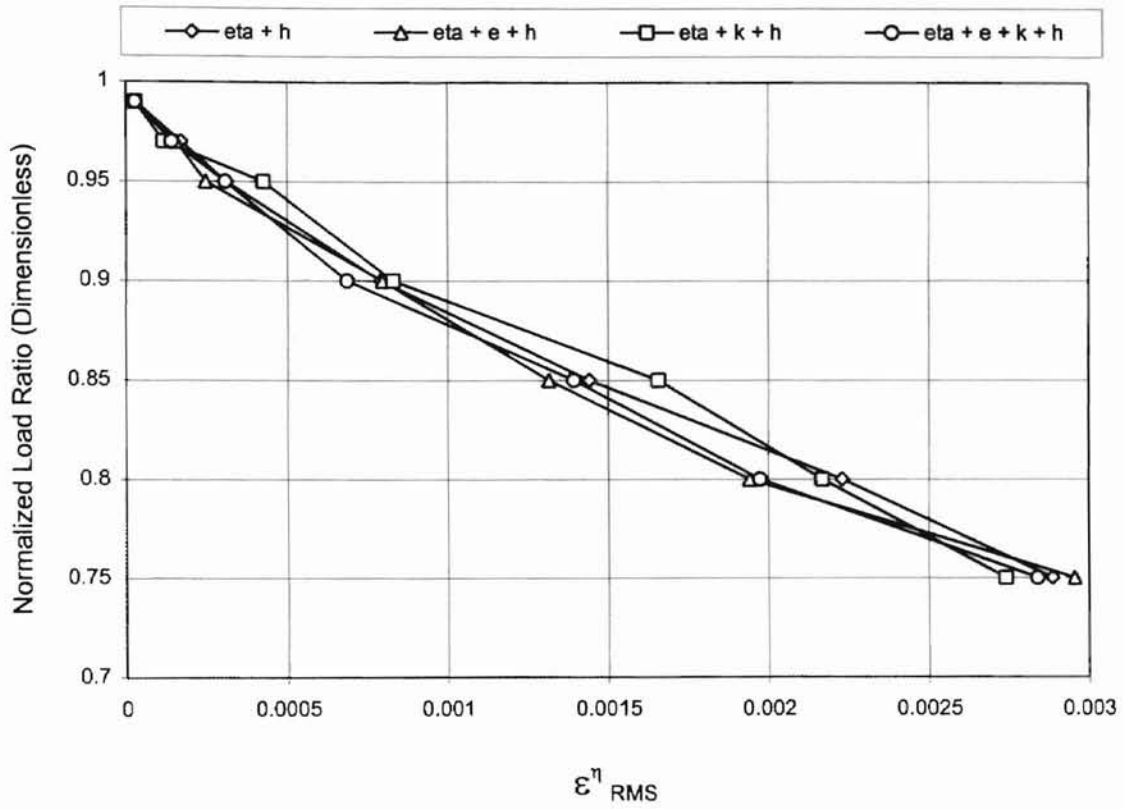
Figure 4.7: η_{SAME}

Effects on eccentricity ε^{η}_{RMS}

Foundation stiffness, $\varphi_o = 225$ Sample size ≈ 50

Eccentricity standard deviation, $\sigma_\eta = 0.05$

All other imperfections: $\kappa_{u_o} = 7.449$, $b_{f_o} = 1.50$, $\sigma_{f_o} = 0.05$

Power spectral density function: $G_{f_o f_o}(\kappa_o) = \frac{1}{2}\sigma_{f_o}^2\, b_{f_o}^3 \kappa_o^2 \exp\left[-b_{f_o}|\kappa_o|\right]$
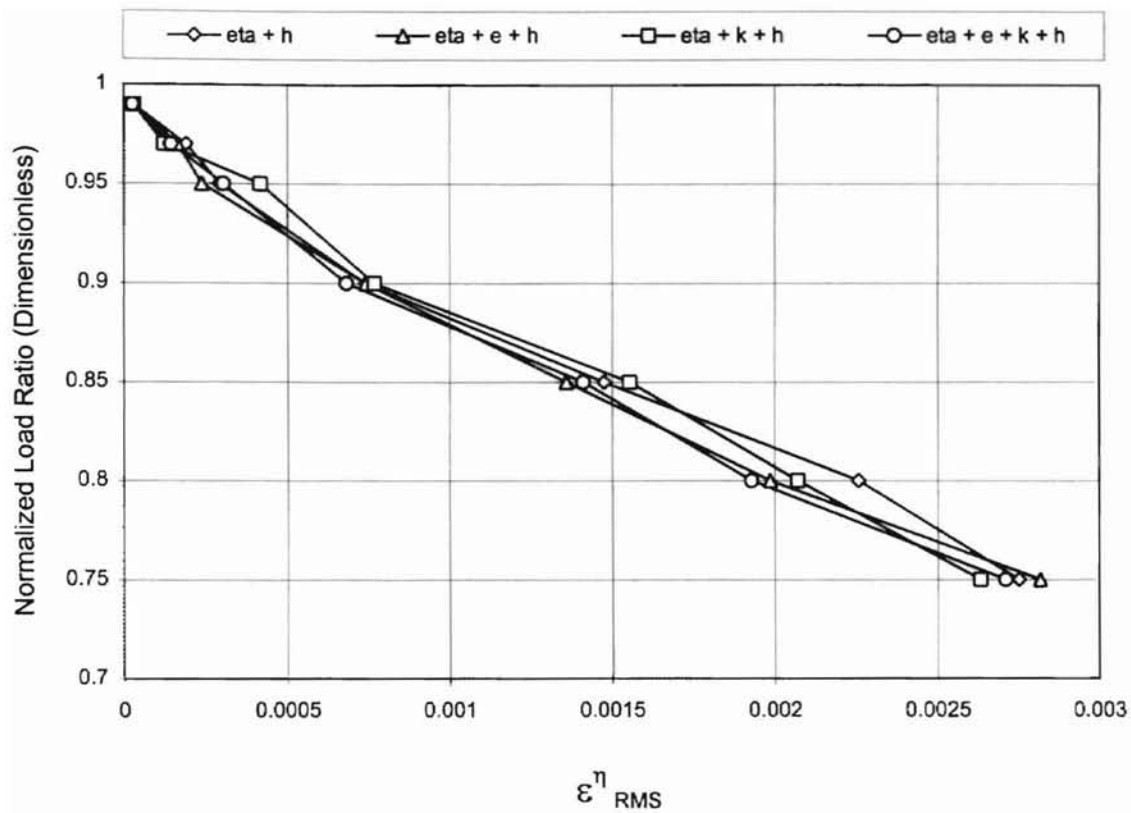
Figure 4.8: η_{OPP}

Effects on eccentricity ε^{η}_{RMS}

Foundation stiffness, $\varphi_o = 225$ Sample size ≈ 50

Eccentricity standard deviation, $\sigma_\eta = 0.05$

All other imperfections: $\kappa_{u_o} = 7.449$, $b_{f_o} = 1.50$, $\sigma_{f_o} = 0.05$

Power spectral density function: $G_{f_o f_o}(\kappa_o) = \frac{1}{2}\sigma_{f_o}^2 b_{f_o}^3 \kappa_o^2 \exp\left[-b_{f_o}|\kappa_o|\right]$

49

Figure 4.9: η_{SAME}
Effects on initial shape $\varepsilon^h{}_{RMS}$

Foundation stiffness, $\varphi_o = 225$ Sample size ≈ 50

Eccentricity standard deviation, $\sigma_\eta = 0.05$

All other imperfections: $\kappa_{u_o} = 7.449$, $b_{f_o} = 1.50$, $\sigma_{f_o} = 0.05$

Power spectral density function: $G_{f_o f_o}(\kappa_o) = \frac{1}{2}\sigma_{f_o}^2 b_{f_o}^3 \kappa_o^2 \exp\left[-b_{f_o}|\kappa_o|\right]$
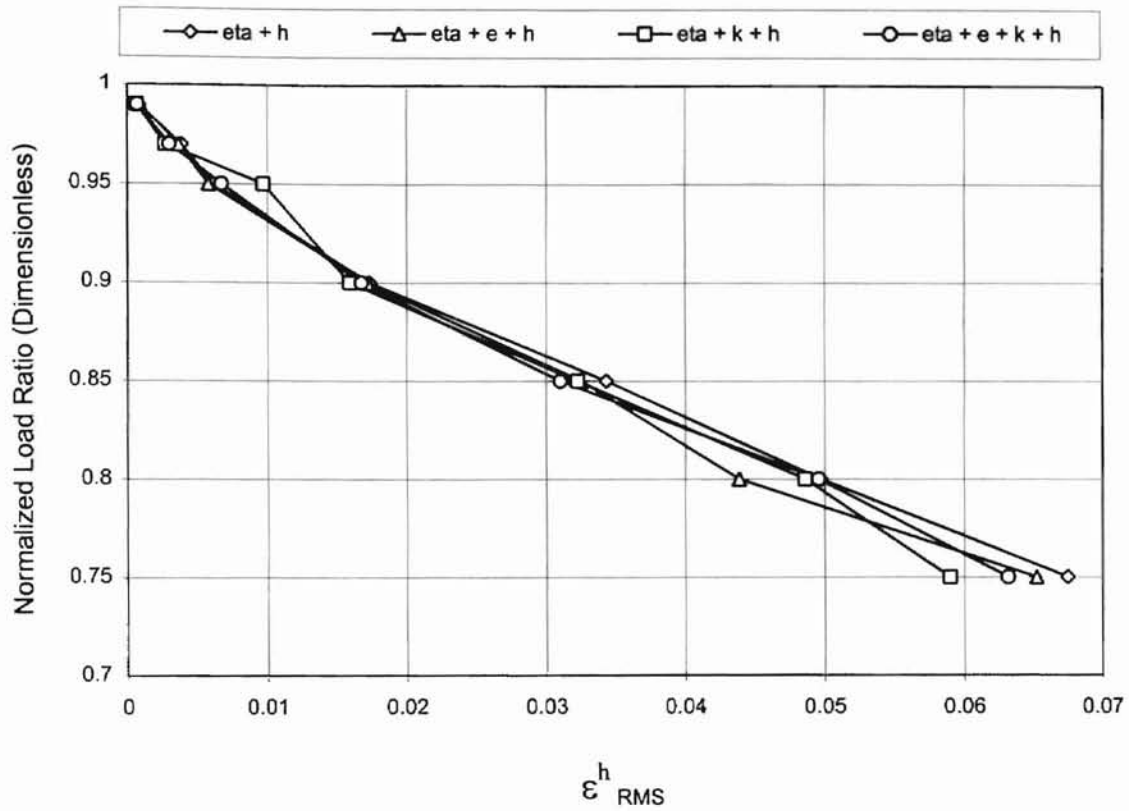
Figure 4.10: η_{OPP}

Effects on initial shape ε^h_{RMS}

Foundation stiffness, $\varphi_o = 225$ Sample size ≈ 50

Eccentricity standard deviation, $\sigma_\eta = 0.05$

All other imperfections: $\kappa_{u_o} = 7.449$, $b_{f_o} = 1.50$, $\sigma_{f_o} = 0.05$

Power spectral density function: $G_{f_o f_o}(\kappa_o) = \frac{1}{2}\sigma_{f_o}^2 b_{f_o}^3 \kappa_o^2 \exp\left[-b_{f_o}|\kappa_o|\right]$
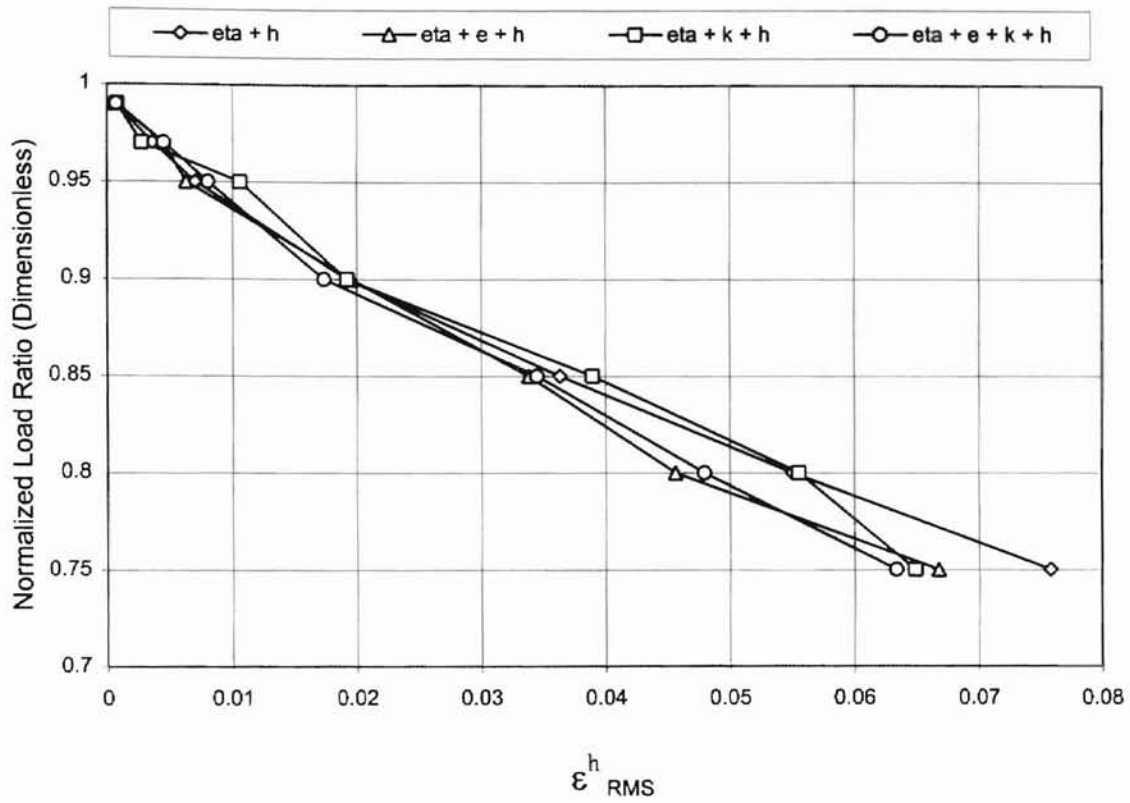
Figure 4.11: η_{SAME}

Effects on bending rigidity $\mathcal{E}^{e}_{RMS}$

Foundation stiffness, $\varphi_o = 225$ Sample size ≈ 50

Eccentricity standard deviation, $\sigma_\eta = 0.05$

All other imperfections: $\kappa_{u_o} = 7.449$, $b_{f_o} = 1.50$, $\sigma_{f_o} = 0.05$

Power spectral density function: $G_{f_o f_o}(\kappa_o) = \frac{1}{2}\sigma^2_{f_o} b^3_{f_o}\kappa^2_o \exp\left[-b_{f_o}|\kappa_o|\right]$
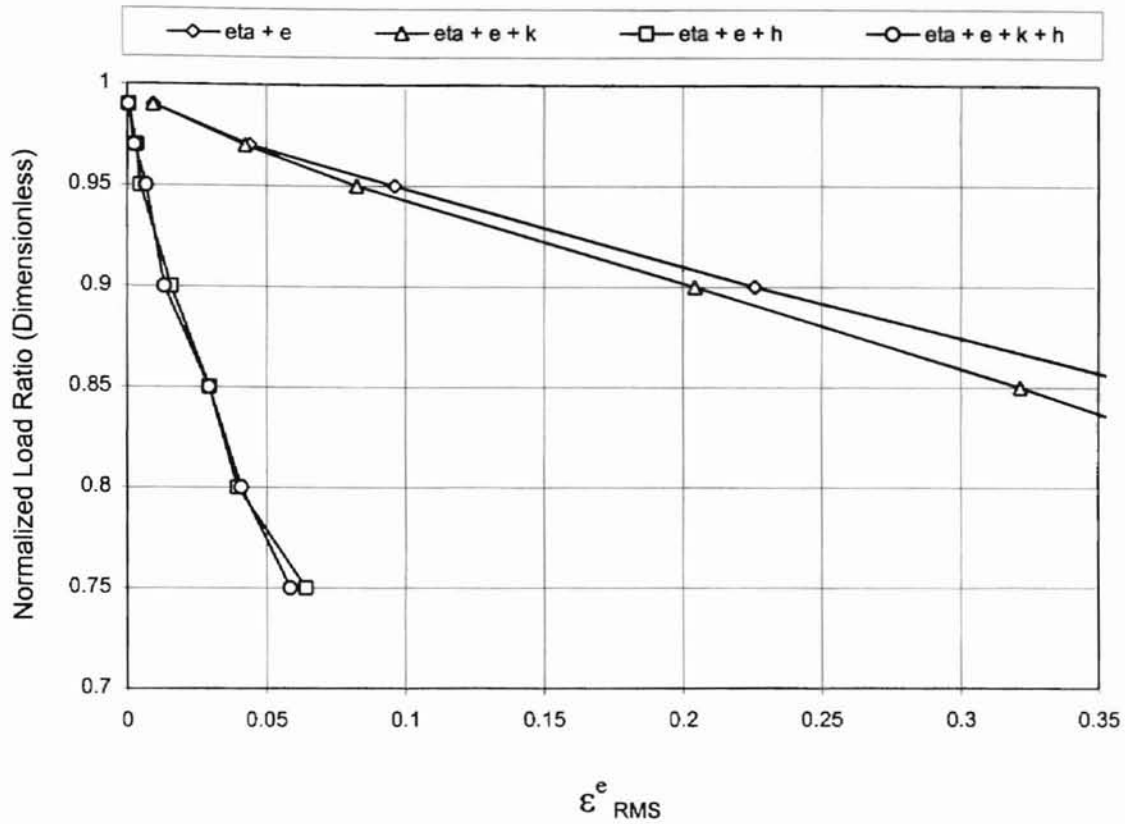
Figure 4.12: η_{OPP}

Effects on bending rigidity ε^e_{RMS}

Foundation stiffness, $\varphi_o = 225$ Sample size ≈ 50

Eccentricity standard deviation, $\sigma_\eta = 0.05$

All other imperfections: $\kappa_{u_o} = 7.449$, $b_{f_o} = 1.50$, $\sigma_{f_o} = 0.05$

Power spectral density function: $G_{f_o f_o}(\kappa_o) = \frac{1}{2}\sigma_{f_o}^2 b_{f_o}^3 \kappa_o^2 \exp\left[-b_{f_o}|\kappa_o|\right]$
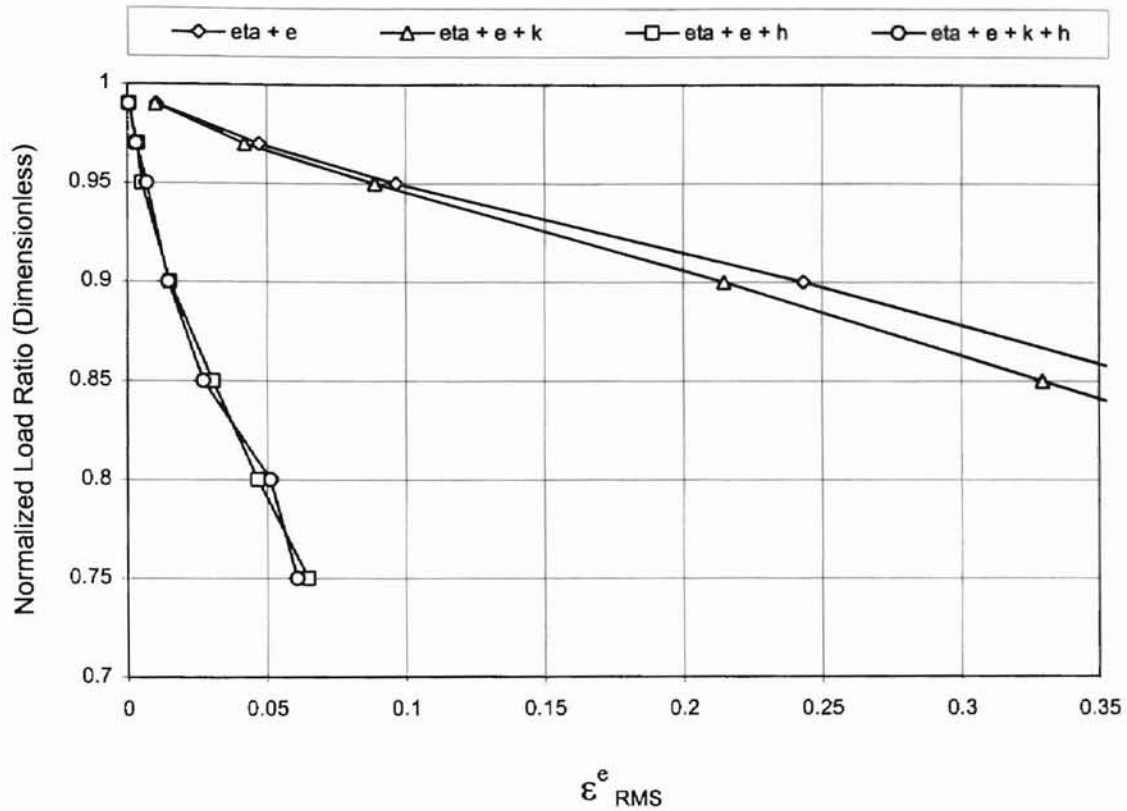
Figure 4.13: η_{SAME}

Effects on foundation stiffness ε^k_{RMS}

Foundation stiffness, $\varphi_o = 225$ Sample size ≈ 50

Eccentricity standard deviation, $\sigma_\eta = 0.05$

All other imperfections: $\kappa_{u_o} = 7.449$, $b_{f_o} = 1.50$, $\sigma_{f_o} = 0.05$

Power spectral density function: $G_{f_o f_o}(\kappa_o) = \frac{1}{2}\sigma^2_{f_o} b^3_{f_o} \kappa^2_o \exp\left[-b_{f_o}|\kappa_o|\right]$
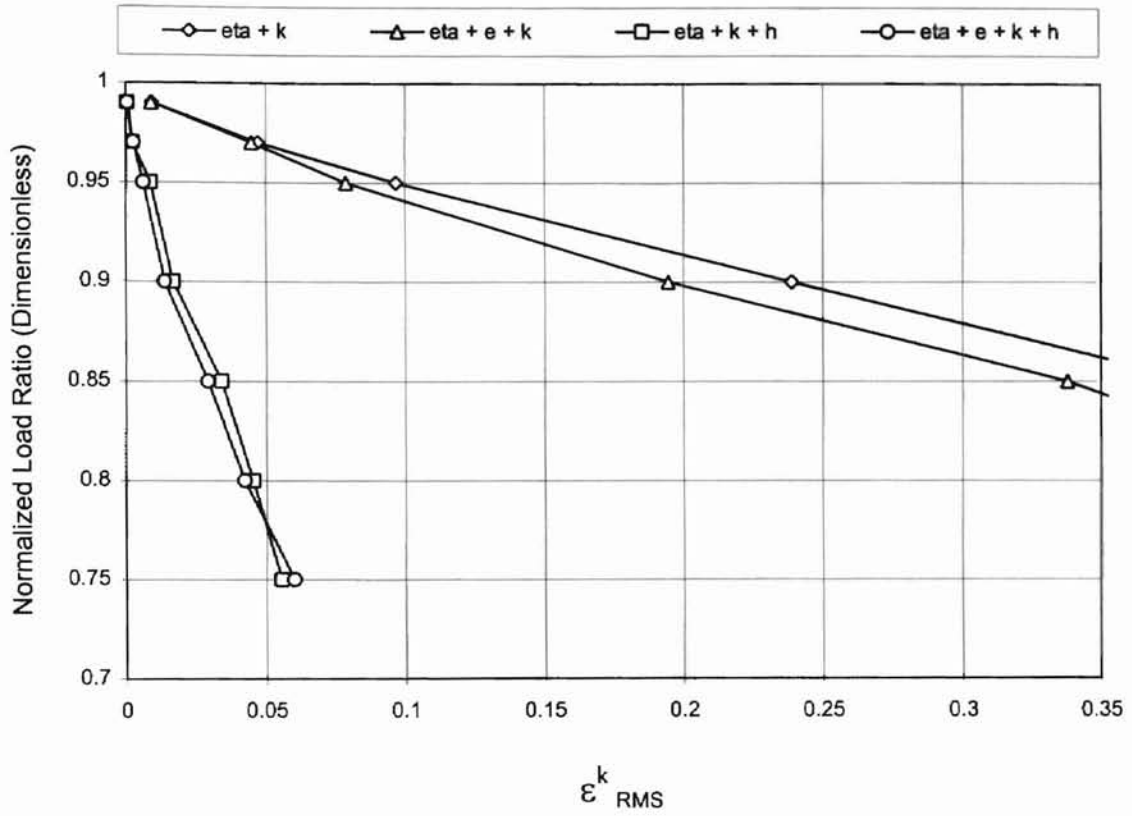
Figure 4.14: η_{OPP}

Effects on foundation stiffness ε^k_{RMS}

Foundation stiffness, $\varphi_o = 225$ Sample size ≈ 50

Eccentricity standard deviation, $\sigma_\eta = 0.05$

All other imperfections: $\kappa_{u_o} = 7.449$, $b_{f_o} = 1.50$, $\sigma_{f_o} = 0.05$

Power spectral density function: $G_{f_o f_o}(\kappa_o) = \frac{1}{2}\sigma^2_{f_o} b^3_{f_o} \kappa^2_o \exp\left[-b_{f_o}|\kappa_o|\right]$
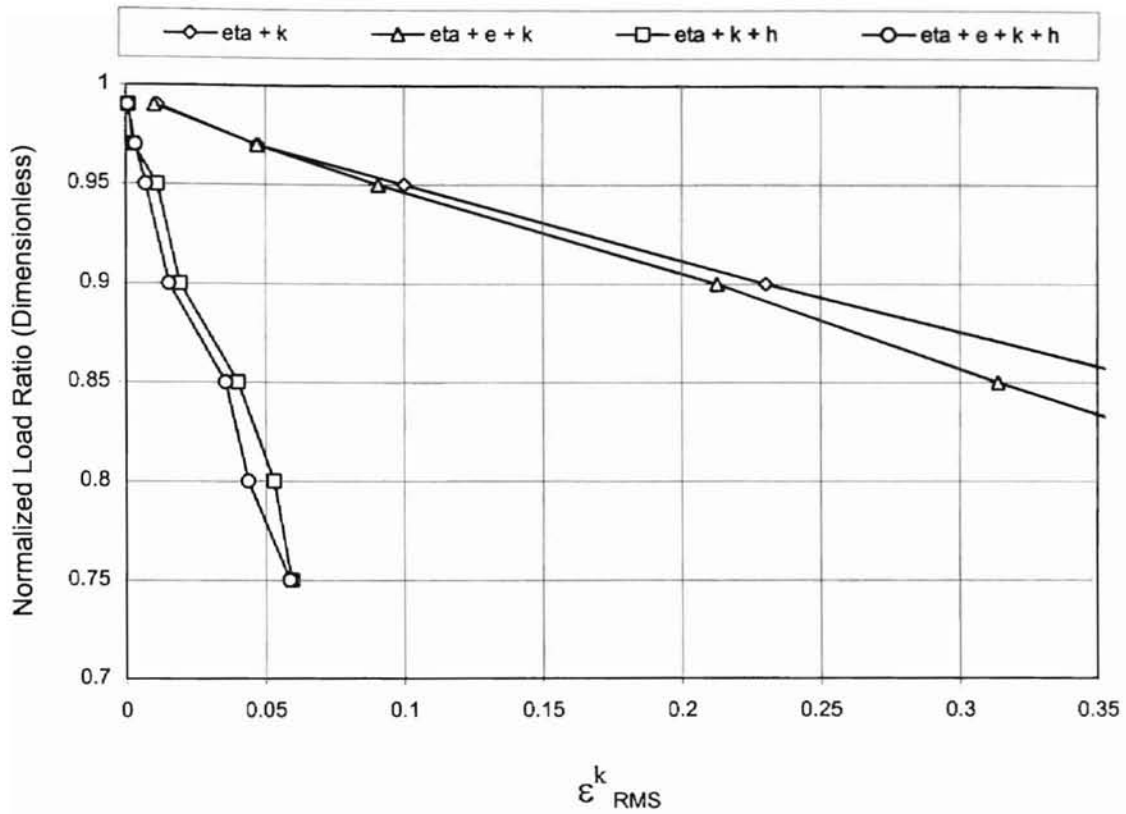
CHAPTER V. *Conclusions*

There are several conclusions that can be drawn from the results of this study.

1. It has been demonstrated for the first time that eccentricity in the applied loads is the most dominant imperfection when the eccentricities are modeled as random variables and the correlation distances for the imperfections in initial shape, bending rigidity, and foundation stiffness are set at reasonable, medium values.

2. It has also been shown that the eccentricity in the applied load is indeed a Type I (shape) imperfection, and that it aggressively interacts with the other Type I imperfection (initial shape) when it too is present.

3. A final result is the observation that there is very little, if any difference in the respective effects of the η_{SAME} and η_{OPP} cases. That is, the absolute magnitude of the end eccentricities are the only parameter of any tangible consequence.

As mentioned throughout this thesis, research on this problem could be extended in a number of ways. Some of the many possible ways include:

1. Use of different power spectral density functions, autocorrelation functions, and appropriate correlation distances.

2. Use of different distributions and statistical parameters for the end eccentricities, such as the uniform and the beta distributions.

3. Remodel the problem using fixed value end eccentricities.

4. Modeling the extensional case of the BEF. This is the case of the BEF whose centerline undergoes shortening (axial strain) prior to buckling.

CIM is a new weapon in the engineer's arsenal. In fact, the exploration of structural mechanics using CIM has only just begun. There is a long, promising road ahead toward a deepening of our understanding of the buckling phenomenon (and it may likely have a few stochastic "bumps" !). This thesis has merely taken a few small steps down that road. With CIM, a great deal of research is now possible.

BIBLIOGRAPHY

Amazigo, J.C., "Buckling of Stochastically Imperfect Structures," *Buckling of Structures*,
B. Budiansky (ed.), 1974.

American Institute of Steel Construction, *Manual of Steel Construction*, American
Institute of Steel Construction, Inc., 1926.

Bazant, Z. and L. Cedolin, *Stability of Structures*, Oxford, 1991.

Elishakoff, I., "Reliability Approach to the Random Imperfection Sensitivity of
Columns," *Acta Mechanica*, v55, 1985.

Elsihakoff, I., "Stochastic Simulation of and Initial Imperfection Data Bank for Isotropic
Shells with General Imperfections," *Buckling of Structures*, I. Elishakoff (ed.),
Elsevier, 1988.

Ivanova, J. and I. Trendafilova, "A Stochastic Approach to the Problem of Stability of a
Spherical Shell with Initial Imperfections," *Probabilistic Engineering Mechanics*, v7,
1992.

Koiter, W.T., *On the Stability of Elastic Equilibrium, Dissertation, Delft, Holland*, 1945.

Langhaar, H. L., *Energy Methods in Applied Mechanics*, Krieger Publishing Co., 1989.

Palassopoulos, G.V., "Response Variability of Structures Subjected to Bifurcation
Buckling," *Journal of Engineering Mechanics*, v118, n6, June 1993.

Press, W.H., Flannery, B.P., Teukolsky, S.A. and W. T. Vetterling, *Numerical Recipes,
the Art of Scientific Computing*, Cambridge, 1989.

Shinozuka, M. and J. Astill, "Random Eigenvalue Problems in Structural Analysis,"
AIAA Journal, v10, 1971.

Shinozuka, M. and G. Deodatis, "Simulation of Stochastic Processes by Spectral Representation," *Applied Mechanics Reviews*, v44, n4, April 1991.

Song, Y. and G.J. Simitses, "Elastoviscoplastic Buckling Behavior of Simply Supported Columns," *AIAA Journal*, v3, n1, January 1992.

Sridharan, S., "Imperfection Sensitivity of Stiffened Cylindrical Shells Under Interactive Buckling," *12th U.S. National Congress of Applied Mechanics*, Seattle, WA 1994.

Thompson, J.M.T. and G.W. Hunt, *A General Theory of Elastic Stability*, Wiley, 1973.

Thompson, J.M.T. and G.W. Hunt, *Elastic Instability Phenomena*, Wiley, 1984.

Timoshenko, S . and J. Gere, *Mechanics of Materials*, PWS-KENT, 1984.

Timoshenko, S. and J. Gere, *Theory of Elastic Stability*, McGraw-Hill, 1961.

Wilson, W.M. and N.M. Newmark, "The Strength of Thin Cylindrical Shells as Columns," *Engineering Experiments Station Bulletin*, U. of Ill., Urbana, Ill., 1933.

Yeigh, B.W., *Imperfections and Instabilities*, *Dissertation*, Princeton, 1995.

APPENDIX

Legend: η =   Eccentricity in the Applied Load

             EI   =   Bending Rigidity

             K   =   Foundation Stiffness

             H   =   Initial Shape

ECCENTRICITIES WITH THE SAME SIGN

$\dfrac{\rho}{\rho_{cl}}$	$\overline{\varepsilon}_{RMS}\,\eta$	$\overline{\varepsilon}_{RMS}\,EI$	$\overline{\varepsilon}_{RMS}\,K$	$\overline{\varepsilon}_{RMS}\,H$
0.99	0.000570	-	-	-
0.97	0.002702	-	-	-
0.95	0.005864	-	-	-
0.90	0.016289	-	-	-
0.85	0.028881	-	-	-
0.80	0.043159	-	-	-
0.75	0.059420	-	-	-

Table A.1: ε_{RMS} (eccentricity) as a function of the normalized load ratio

ECCENTRICITIES WITH OPPOSITE SIGNS

$\dfrac{\rho}{\rho_{cl}}$	$\overline{\varepsilon}_{RMS}\,\eta$	$\overline{\varepsilon}_{RMS}\,EI$	$\overline{\varepsilon}_{RMS}\,K$	$\overline{\varepsilon}_{RMS}\,H$
0.99	0.000478	-	-	-
0.97	0.002577	-	-	-
0.95	0.005669	-	-	-
0.90	0.016144	-	-	-
0.85	0.028976	-	-	-
0.80	0.043551	-	-	-
0.75	0.059954	-	-	-

Table A.2: ε_{RMS} (eccentricity) as a function of the normalized load ratio

Foundation stiffness: $\varphi_o = 225$ Sample Size ≈ 50

For eccentricity in the applied load : $\sigma_\eta = 0.05$

ECCENTRICITIES WITH THE SAME SIGN

$\dfrac{\rho}{\rho_{cl}}$	$\bar{\varepsilon}_{RMS}\,\eta$	$\bar{\varepsilon}_{RMS}\,EI$	$\bar{\varepsilon}_{RMS}\,K$	$\bar{\varepsilon}_{RMS}\,H$
0.99	0.000463	0.006451	-	-
0.97	0.002321	0.044168	-	-
0.95	0.004619	0.096359	-	-
0.90	0.011522	0.226110	-	-
0.85	0.018380	0.370480	-	-
0.80	0.025982	0.502930	-	-
0.75	0.031236	0.592930	-	-

Table A.3: ε_{RMS} (eccentricity and bending rigidity) as a function of the normalized load ratio

ECCENTRICITIES WITH THE OPPOSITE SIGN

$\dfrac{\rho}{\rho_{cl}}$	$\bar{\varepsilon}_{RMS}\,\eta$	$\bar{\varepsilon}_{RMS}\,EI$	$\bar{\varepsilon}_{RMS}\,K$	$\bar{\varepsilon}_{RMS}\,H$
0.99	0.000419	0.010520	-	-
0.97	0.002137	0.047239	-	-
0.95	0.004423	0.096790	-	-
0.90	0.010737	0.243460	-	-
0.85	0.018371	0.372610	-	-
0.80	0.023717	0.506760	-	-
0.75	0.033082	0.603000	-	-

Table A.4: ε_{RMS} (eccentricity and bending rigidity) as a function of the normalized load ratio

Foundation stiffness: $\quad\quad\quad\quad \varphi_o = 225 \quad\quad\quad\quad$ Sample Size ≈ 50

For eccentricity in the applied load : $\quad \sigma_\eta = 0.05$

For all other imperfections: $\quad\quad\quad \kappa_{uo} = 7.449,\ b_{fo} = 1.50,\ \sigma_{fo} = 0.05$

Power spectral density function: $\quad\quad G_{f_o f_o}(\kappa_o) = \dfrac{1}{2}\sigma_{f_o}^2\,b_{f_o}^3\,\kappa_o^2\,\exp\left[-b_{f_o}|\kappa_o|\right]$

ECCENTRICITIES WITH THE SAME SIGN

$\dfrac{\rho}{\rho_{cl}}$	$\overline{\varepsilon}_{RMS}\,\eta$	$\overline{\varepsilon}_{RMS}\,EI$	$\overline{\varepsilon}_{RMS}\,K$	$\overline{\varepsilon}_{RMS}\,H$
0.99	0.000444	-	0.009337	-
0.97	0.022755	-	0.047256	-
0.95	0.004357	-	0.096852	-
0.90	0.011787	-	0.238930	-
0.85	0.020744	-	0.385010	-
0.80	0.029758	-	0.512430	-
0.75	0.036209	-	0.663800	-

Table A.5: ε_{RMS} (eccentricity and foundation stiffness) as a function of the normalized load ratio

ECCENTRICITIES WITH OPPOSITE SIGNS

$\dfrac{\rho}{\rho_{cl}}$	$\overline{\varepsilon}_{RMS}\,\eta$	$\overline{\varepsilon}_{RMS}\,EI$	$\overline{\varepsilon}_{RMS}\,K$	$\overline{\varepsilon}_{RMS}\,H$
0.99	0.000440	-	0.011346	-
0.97	0.002179	-	0.047153	-
0.95	0.004419	-	0.100220	-
0.90	0.10951	-	0.230450	-
0.85	0.18495	-	0.373310	-
0.80	0.26075	-	0.546170	-
0.75	0.33239	-	0.675870	-

Table A.6: ε_{RMS} (eccentricity and foundation stiffness) as a function of the normalized load ratio

Foundation stiffness: $\varphi_o = 225$ Sample Size ≈ 50

For eccentricity in the applied load : $\sigma_\eta = 0.05$

For all other imperfections: $\kappa_{uo} = 7.449,\ b_{fo} = 1.50,\ \sigma_{fo} = 0.05$

Power spectral density function: $G_{f_o f_o}(\kappa_o) = \dfrac{1}{2}\sigma_{f_o}^2\, b_{f_o}^3\, \kappa_o^2 \exp\!\left[-b_{f_o}|\kappa_o|\right]$

ECCENTRICITIES WITH THE SAME SIGN

$\dfrac{\rho}{\rho_{cl}}$	$\overline{\varepsilon}_{RMS}\,\eta$	$\overline{\varepsilon}_{RMS}\,EI$	$\overline{\varepsilon}_{RMS}\,K$	$\overline{\varepsilon}_{RMS}\,H$
0.99	0.000030	-	-	0.000797
0.97	0.000170	-	-	0.003867
0.95	0.000311	-	-	0.006135
0.90	0.000793	-	-	0.017387
0.85	0.001443	-	-	0.034349
0.80	0.002230	-	-	0.049733
0.75	0.002886	-	-	0.067470

Table A.7: ε_{RMS} (eccentricity and shape) as a function of the normalized load ratio

ECCENTRICITIES WITH OPPOSITE SIGNS

$\dfrac{\rho}{\rho_{cl}}$	$\overline{\varepsilon}_{RMS}\,\eta$	$\overline{\varepsilon}_{RMS}\,EI$	$\overline{\varepsilon}_{RMS}\,K$	$\overline{\varepsilon}_{RMS}\,H$
0.99	0.000028	-	-	0.000680
0.97	0.000190	-	-	0.003612
0.95	0.000292	-	-	0.007052
0.90	0.000742	-	-	0.019297
0.85	0.001476	-	-	0.036353
0.80	0.002258	-	-	0.055068
0.75	0.002750	-	-	0.075804

Table A.8: ε_{RMS} (eccentricity and shape) as a function of the normalized load ratio

Foundation stiffness: $\qquad$ $\varphi_o = 225$ $\qquad\qquad$ Sample Size ≈ 50

For eccentricity in the applied load : $\sigma_\eta = 0.05$

For all other imperfections: $\qquad$ $\kappa_{uo} = 7.449$, $b_{fo} = 1.50$, $\sigma_{fo} = 0.05$

Power spectral density function: $\qquad$ $G_{f_o f_o}(\kappa_o) = \dfrac{1}{2}\sigma_{f_o}^2\, b_{f_o}^3\, \kappa_o^2 \exp\left[-b_{f_o}|\kappa_o|\right]$

ECCENTRICITIES WITH THE SAME SIGN

$\dfrac{\rho}{\rho_{cl}}$	$\bar{\varepsilon}_{RMS}\,\eta$	$\bar{\varepsilon}_{RMS}\,EI$	$\bar{\varepsilon}_{RMS}\,K$	$\bar{\varepsilon}_{RMS}\,H$
0.99	0.000438	0.009275	0.009020	-
0.97	0.002249	0.042398	0.044941	-
0.95	0.004282	0.082628	0.078859	-
0.90	0.010483	0.204490	0.194560	-
0.85	0.016071	0.321560	0.337900	-
0.80	0.022154	0.429940	0.437190	-
0.75	0.027526	0.565970	0.508020	-

Table A.9: ε_{RMS} (eccentricity, bending rigidity, and foundation stiffness)
as a function of the normalized load ratio

ECCENTRICITIES WITH OPPOSITE SIGNS

$\dfrac{\rho}{\rho_{cl}}$	$\bar{\varepsilon}_{RMS}\,\eta$	$\bar{\varepsilon}_{RMS}\,EI$	$\bar{\varepsilon}_{RMS}\,K$	$\bar{\varepsilon}_{RMS}\,H$
0.99	0.000423	0.010102	0.010171	-
0.97	0.002042	0.042061	0.047078	-
0.95	0.003953	0.089051	0.090854	-
0.90	0.009578	0.214770	0.212800	-
0.85	0.16029	0.329370	0.313850	-
0.80	0.020801	0.446230	0.425480	-
0.75	0.023660	0.486610	0.494460	-

Table A.10: ε_{RMS} (eccentricity, bending rigidity, and foundation stiffness)
as a function of the normalized load ratio

Foundation stiffness: $\varphi_o = 225$ Sample Size ≈ 50

For eccentricity in the applied load : $\sigma_\eta = 0.05$

For all other imperfections: $\kappa_{uo} = 7.449,\ b_{fo} = 1.50,\ \sigma_{fo} = 0.05$

Power spectral density function: $G_{f_o f_o}(\kappa_o) = \dfrac{1}{2}\sigma_{f_o}^2\, b_{f_o}^3\, \kappa_o^2 \exp\!\left[-b_{f_o}|\kappa_o|\right]$

ECCENTRICITIES WITH THE SAME SIGN

$\dfrac{\rho}{\rho_{cl}}$	$\bar{\varepsilon}_{RMS}\,\eta$	$\bar{\varepsilon}_{RMS}\,EI$	$\bar{\varepsilon}_{RMS}\,K$	$\bar{\varepsilon}_{RMS}\,H$
0.99	0.000031	0.000666	-	0.000886
0.97	0.000155	0.003358	-	0.003652
0.95	0.000247	0.004760	-	0.005788
0.90	0.000798	0.015696	-	0.017239
0.85	0.001316	0.029342	-	0.032533
0.80	0.001942	0.039546	-	0.043878
0.75	0.002956	0.064171	-	0.065212

Table A.11: ε_{RMS} (eccentricity, bending rigitity, and shape)
as a function of the normalized load ratio

ECCENTRICITIES WITH OPPOSITE SIGNS

$\dfrac{\rho}{\rho_{cl}}$	$\bar{\varepsilon}_{RMS}\,\eta$	$\bar{\varepsilon}_{RMS}\,EI$	$\bar{\varepsilon}_{RMS}\,K$	$\bar{\varepsilon}_{RMS}\,H$
0.99	0.000029	0.000689	-	0.000679
0.97	0.000164	0.003601	-	0.004475
0.95	0.000238	0.005279	-	0.006295
0.90	0.000742	0.015152	-	0.019615
0.85	0.001361	0.030511	-	0.033860
0.80	0.001986	0.046695	-	0.045648
0.75	0.002816	0.064907	-	0.066776

Table A.12: ε_{RMS} (eccentricity, bending rigidity, and shape)
as a function of the normalized load ratio

Foundation stiffness: $\qquad\qquad \varphi_o = 225 \qquad\qquad$ Sample Size ≈ 50

For eccentricity in the applied load : $\sigma_\eta = 0.05$

For all other imperfections: $\qquad\quad \kappa_{uo} = 7.449,\ b_{fo} = 1.50,\ \sigma_{fo} = 0.05$

Power spectral density function: $\qquad G_{f_o f_o}(\kappa_o) = \dfrac{1}{2}\sigma_{f_o}^2\,b_{f_o}^3\,\kappa_o^2\,\exp\left[-b_{f_o}|\kappa_o|\right]$

ECCENTRICITIES WITH THE SAME SIGN

$\dfrac{\rho}{\rho_{cl}}$	$\bar{\varepsilon}_{RMS}\,\eta$	$\bar{\varepsilon}_{RMS}\,EI$	$\bar{\varepsilon}_{RMS}\,K$	$\bar{\varepsilon}_{RMS}\,H$
0.99	0.000028	-	0.000593	0.000654
0.97	0.000118	-	0.002298	0.002695
0.95	0.000427	-	0.008799	0.009739
0.90	0.000831	-	0.016805	0.015966
0.85	0.001657	-	0.034152	0.032286
0.80	0.002169	-	0.045416	0.048626
0.75	0.002740	-	0.055573	0.058996

Table A.13: ε_{RMS} (eccentricity, foundation stiffness, and shape)
as a function of the normalized load ratio

ECCENTRICITIES WITH OPPOSITE SIGNS

$\dfrac{\rho}{\rho_{cl}}$	$\bar{\varepsilon}_{RMS}\,\eta$	$\bar{\varepsilon}_{RMS}\,EI$	$\bar{\varepsilon}_{RMS}\,K$	$\bar{\varepsilon}_{RMS}\,H$
0.99	0.000030	-	0.000812	0.000787
0.97	0.000123	-	0.002526	0.002744
0.95	0.000418	-	0.011215	0.010646
0.90	0.000769	-	0.019308	0.019249
0.85	0.001556	-	0.040041	0.038977
0.80	0.002071	-	0.053058	0.055579
0.75	0.002632	-	0.059405	0.064906

Table A.14: ε_{RMS} (eccentricity, foundation stiffness, and shape)
as a function of the normalized load ratio

Foundation stiffness: $\varphi_o = 225$ Sample Size ≈ 50

For eccentricity in the applied load : $\sigma_\eta = 0.05$

For all other imperfections: $\kappa_{uo} = 7.449,\ b_{fo} = 1.50,\ \sigma_{fo} = 0.05$

Power spectral density function: $G_{f_o f_o}(\kappa_o) = \dfrac{1}{2}\sigma_{f_o}^2\, b_{f_o}^3\, \kappa_o^2\, \exp\left[-b_{f_o}\left|\kappa_o\right|\right]$

ECCENTRICITIES WITH THE SAME SIGN

$\dfrac{\rho}{\rho_{cl}}$	$\overline{\varepsilon}_{RMS}\,\eta$	$\overline{\varepsilon}_{RMS}\,EI$	$\overline{\varepsilon}_{RMS}\,K$	$\overline{\varepsilon}_{RMS}\,H$
0.99	0.000029	0.000617	0.000652	0.000720
0.97	0.000142	0.002628	0.002772	0.002990
0.95	0.000309	0.006893	0.006292	0.006732
0.90	0.000688	0.013316	0.013772	0.016815
0.85	0.001395	0.029300	0.029244	0.031053
0.80	0.001975	0.040900	0.042334	0.049591
0.75	0.002840	0.058591	0.060221	0.063173

Table A.15: ε_{RMS} (eccentricity, bending rigidity, foundation stiffness, and shape)
as a function of the normalized load ratio

ECCENTRICITIES WITH OPPOSITE SIGNS

$\dfrac{\rho}{\rho_{cl}}$	$\overline{\varepsilon}_{RMS}\,\eta$	$\overline{\varepsilon}_{RMS}\,EI$	$\overline{\varepsilon}_{RMS}\,K$	$\overline{\varepsilon}_{RMS}\,H$
0.99	0.000027	0.000755	0.000659	0.000763
0.97	0.000144	0.003203	0.003362	0.004523
0.95	0.000304	0.007017	0.007066	0.008172
0.90	0.000683	0.014678	0.015423	0.017433
0.85	0.001412	0.027097	0.035577	0.034545
0.80	0.001930	0.051241	0.043793	0.047989
0.75	0.002710	0.060895	0.058833	0.063419

Table A.16: ε_{RMS} (eccentricity, bending rigidity, foundation stiffnes and shape)
as a function of the normalized load ratio

Foundation stiffness: $\qquad\qquad\qquad \varphi_o = 225 \qquad\qquad$ Sample Size ≈ 50

For eccentricity in the applied load : $\sigma_\eta = 0.05$

For all other imperfections: $\qquad\quad \kappa_{uo} = 7.449,\ b_{fo} = 1.50,\ \sigma_{fo} = 0.05$

Power spectral density function: $\qquad G_{f_o f_o}(\kappa_o) = \dfrac{1}{2}\sigma_{f_o}^2\, b_{f_o}^3\, \kappa_o^2\, \exp\!\left[-b_{f_o}|\kappa_o|\right]$

VITA

James Alan Hoffman

Candidate for the Degree of

Master of Science

Thesis: STABILITY OF STRUCTURES SUBJECTED TO ECCENTRIC LOAD
IMPERFECTIONS

Major Field: Civil Engineering

Biographical:

Personal Data: Born in Tulsa, Oklahoma, on November 19, 1966, the son of Joe and
Betty Hoffman. Married to Stacy Ann Hoffman (*nee* Wilkerson) on August 6,
1994.

Educational Data: Graduated from Street School/Project 12, Tulsa, Oklahoma in May
1985; received Associate of Science Degree in Engineering from Tulsa Junior
College, Tulsa, Oklahoma, July 1991; received Bachelor of Science Degree in
Civil Engineering from Oklahoma State University, Stillwater, Oklahoma in
May 1994; Completed the requirements for the Master of Science Degree with a
major in Civil Engineering at Oklahoma State University in December 1996.

Experience: Employed by Steel and Pipe Supply Company as a crane operator, Port
of Catoosa, Oklahoma, 1985 to 1987. Employed by Oklahoma Fixture
Company as a millman/carpenter, Tulsa, Oklahoma, 1987 to 1988. Employed by
Oklahoma State University as an undergraduate teaching assistant; Oklahoma
State University, Department of Civil and Environmental Engineering, 1993 to
1994. Employed with Sturm Engineering Company in Oklahoma City,
Oklahoma since May 1994.

Professional Memberships: Oklahoma Structural Engineers Association (charter
member), American Concrete Institute.